

## Article

# Pollution and Risk Evaluation of Toxic Metals and Metalloid in Water Resources of San Jose, Occidental Mindoro, Philippines

Delia B. Senoro <sup>1,2,3,4,\*</sup>, Kevin Lawrence M. De Jesus <sup>1,2,4</sup> and Cris Edward F. Monjardin <sup>1,2,3,4,5</sup>

<sup>1</sup> Resiliency and Sustainable Development Center, Yuchengco Innovation Center, Mapua University, Intramuros, Manila 1002, Philippines

<sup>2</sup> School of Graduate Studies, Mapua University, Intramuros, Manila 1002, Philippines

<sup>3</sup> School of Civil, Environmental, and Geological Engineering, Mapua University, Intramuros, Manila 1002, Philippines

<sup>4</sup> School of Chemical, Biological, Materials Engineering and Sciences, Mapua University, Intramuros, Manila 1002, Philippines

<sup>5</sup> Department of Civil and Environmental Engineering, Spencer Engineering Building, University of Western Ontario, London, ON N6A 3K7, Canada

\* Correspondence: dbsenoro@mapua.edu.ph; Tel.: + 63-2-8251-6622

**Abstract:** Clean and safe drinking water is an integral part of daily living and is considered as a basic human need. Hence, this study investigated the suitability of the domestic water (DW) and groundwater (GW) samples with respect to the presence of metals and metalloid (MMs) in San Jose, Occidental Mindoro, Philippines. The MMs analyzed in the area of study for DW and GW were Arsenic (As), Barium (Ba), Copper (Cu), Chromium (Cr), Iron (Fe), Lead (Pb), Manganese (Mn), Nickel (Ni), and Zinc (Zn). The results revealed that Pb has the mean highest concentration for DW, while Fe is in GW resources in the area. Quality evaluation of DW and GW was performed using Metal Pollution Index (MPI), Nemerow's Pollution Index (NPI), and Ecological Risk Index (ERI). The mean NPI value calculated for DW was 135 times greater than the upper limit of the unpolluted location category. The highest NPI observed was 1080 times higher than the upper limit of the unpolluted site category. That of the ERI observed in the area was 23.8 times higher than the upper limit for a "low" ERI category. Furthermore, the health risk assessment (HRA) of the GW and DW of the study area revealed non-carcinogenic health risks of the MMs analyzed in GW samples, and potential carcinogenic health risks from As, Cr, Pb, and Ni in DW. The use of machine learning geostatistical interpolation (MLGI) mapping to illustrate the PI and health risk (HR) in the area was an efficient and dependable evaluation tool for assessing and identifying probable MMs pollution hotspots. The data, tools, and the process could be utilized in carrying out water assessment, the evaluation leading to a comprehensive water management program in the area and neighboring regions of similar conditions.

**Keywords:** metals and metalloid; pollution index; ecological risk; health risk; spatial analysis

**Citation:** Senoro, D.B.; De Jesus, K.L.M.; Monjardin, C.E.F. Pollution and Risk Evaluation of Toxic Metals and Metalloid in Water Resources of San Jose, Occidental Mindoro, Philippines. *Sustainability* **2023**, *15*, 3667. <https://doi.org/10.3390/su15043667>

Academic Editor: Said Muhammad

Received: 25 January 2023

Revised: 12 February 2023

Accepted: 13 February 2023

Published: 16 February 2023



**Copyright:** © 2023 by the authors. Licensee MDPI, Basel, Switzerland. This article is an open access article distributed under the terms and conditions of the Creative Commons Attribution (CC BY) license (<https://creativecommons.org/licenses/by/4.0/>).

## 1. Introduction

Water is fundamental in sustaining the quality of life in a community, as it is also attributed to the health, food, and economy of the area. Sustainable Development Goal 6 intends to guarantee the access of all people to clean and affordable water sources, especially those in remote areas. However, due to continuous changes in the landscape, land use, and anthropogenic processes, water resources have been compromised, which poses a threat to the people in the nearby communities, especially in remote regions, since these water resources are the only source for domestic and agricultural activities [1]. Due to its possible toxicity and probable health adverse effects, metals and metalloid (MMs) contamination in water resources are of paramount concern. The pollution of water resources is a result of either natural processes, such as weathering of rocks and runoff, or

anthropogenic activities, such as mining, industrial, and agricultural activities. A hazardous concentration of MMs could build up and have negative consequences on the environment and human health. As their concentrations increase, these MMs may cause more harm to the environment and water systems. When water supplies and the ecosystem are poisoned with high amounts of MMs, health issues and consequences are imminent [2,3]. The quality of drinking and irrigation water supplies declines as a result of MMs migration to water resources. Furthermore, a high concentration of MMs from both anthropogenic and natural sources has a detrimental effect on domestic water (DW) quality [4]. The DW is defined as water used by the population for drinking, cooking, and bathing. The list of abbreviations and symbols used in this study is presented in Abbreviations Section.

The MMs that are naturally present in the earth's crust are transferred into water resources through weathering and decomposition of metal rock and ores, whereas MMs from anthropogenic activities are released through automobile emissions, improper management of waste, the burning of fossil fuels, the usage of fertilizer and pesticides, untreated wastewater, and atmospheric precipitation from mineral extraction, metal processing, and agricultural operations [5]. Investigations of water quality have been conducted on a regional scale to evaluate the current state of the water resources in reference to the MMs present in the area [6,7]. Table A1 in Appendix A enumerates the MMs pollution and health risk assessment (HRA) studies in various regions of the world.

The HRA is a valuable instrument to assess and appraise the probability of health effects with respect to MMs [8]. The elevated concentrations of arsenic (As) [9], barium (Ba) [10], and manganese (Mn) [11] have adverse effects on human health. Metals like copper (Cu), iron (Fe), nickel (Ni), and zinc (Zn) are necessary for the regular growth and functioning of living organisms [12]; however, excess amounts will lead to adverse health effects, too.

The use of GIS to further reinforce the calculated pollution index and health risks has been implemented to several DW and environmental monitoring studies, including MMs in shallow GW in a lake plain in China [13]; MPI of GW in a city in India [14]; HEI and HRA in a GW plain in Iran [15]; WQI, MPI, and PI in a surface water body in Egypt [16]; WQI, MPI, HEI, and HRA in a river and stream in Turkey [17,18]; and WQI, HPI, HEI, and HRA and identification of pollution hotspots in a river in Ethiopia [19]. A good knowledge of the geochemical origin of the pollutants in water resources was obtained by the mapping of the MMs concentration and associated risk indices [20].

Domestic water quality monitoring with respect to MMs concentration has been a challenge in the Philippines due to several factors such as: cost of portable devices used for on-site detection and analysis, laboratory fees for MMs tests and analysis, proximity of sampling sites to the capable laboratory, limited number of laboratories capable of conducting MMs detection and analysis, and government permits to purchase instruments calibration standard solutions, among related others. In the province of Occidental Mindoro, only a limited number of research works have been carried out to detect and analyze MMs in DW and create spatial concentration maps of MMs and their associated indices that can identify pollution hotspots. Hence, the current work investigated the suitability of the water resources in the municipality of San Jose province of Occidental Mindoro, Philippines for domestic consumption, evaluated the risks of possible pollution, and created spatial distribution maps to determine the pollution hotspots. This is with respect to and degree of concentrations of metalloid arsenic (As) and metals such as Ba, Cu, chromium (Cr), Fe, lead (Pb), Mn, Ni, and Zn. The outcomes of this research offer additional data on the existence of MMs in DW resources and help locals create preventive measures, as well as allowing for environmental health professionals to lessen the adverse impacts of MMs in the water resources. It can also be used as a source of data and benchmark activities to create strategic programs to mitigate the presence of elevated MMs concentrations in the Philippines and other neighboring regions.

The DW is basically the potable freshwater that each household uses for everyday needs. However, due to some malpractices and lack of knowledge, unintentional

contamination occurs. The DW is supplied by utility companies that have extracted water underground, as well as some from surface water, but have done traditional treatment before distribution to households and commercial establishments. Some households have their own shallow well for their DW needs.

## 2. Materials and Methods

### 2.1. Description of the Study Area

The municipality of San Jose is a coastal municipality in the province of Occidental Mindoro, in which the municipal center is located at 12°21' N, 121°4' E with an average natural grade line (ground) elevation of 7.8 m above mean sea level. The municipality has a total land area of 446.70 km<sup>2</sup>, which is 7.63% of the total area of the province of Occidental Mindoro [21]. Geographically, San Jose is 173 km from the municipality of Mamburao, the capital city of the province. The municipalities of Rizal and Calintaan, Mansalay, Bulalacao, Magsaysay, and the Mindoro Strait form the northern, eastern, southern, and western borders of San Jose, respectively [22]. The map of the study area is presented as Figure 1.

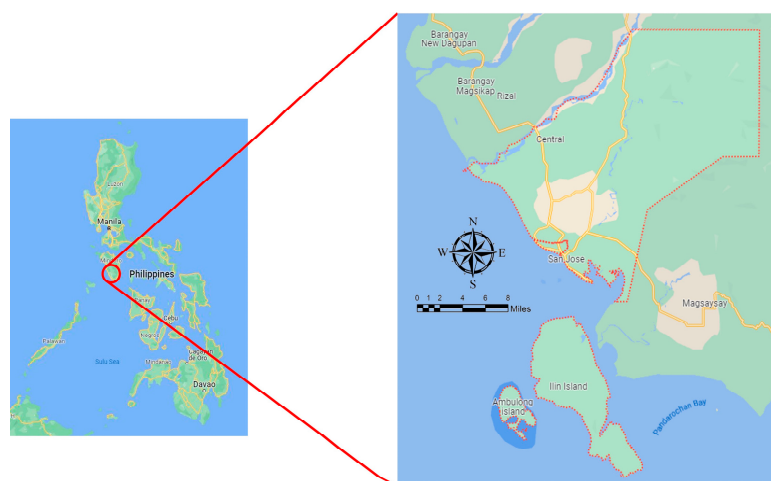


**Figure 1.** Area of the study.

Based on the 2020 census, the total population of the San Jose municipality was 153,267, which constitutes of 29.17% of the total population of the province. San Jose is comprised of 39 barangays (the smallest administrative unit of the local government), with Barangay San Roque as the most populous barangay with 10.26% of the total population of the municipality [23]. The climate in Occidental Mindoro is Type I, with two distinct seasons. The weather is dry from November to April and rainy the rest of the year [24] with runoff that contributes to the pollution of water resources.

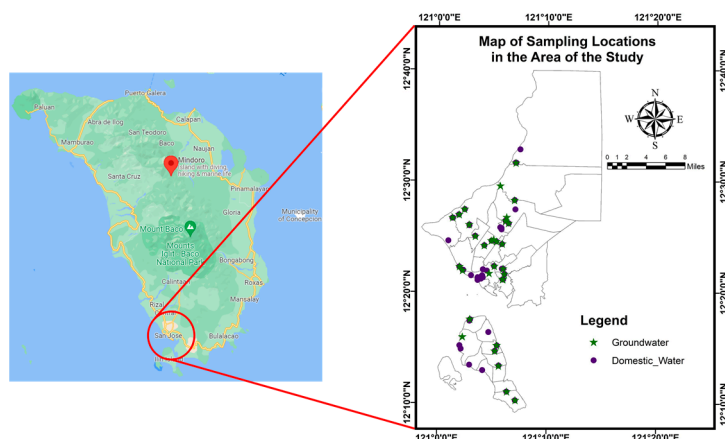
A total of 11 rivers and creeks cut through the town, creating a network that also acts as a natural drainage system. A tributary river system to the Busuanga River exists in the region and is the primary source of irrigation for agricultural land. The barangays of San Jose are divided among four watersheds on the mainland and one on an island, with a combined size of around 626.2 km<sup>2</sup>. These watersheds are Busuanga, Cabariwan, Caguray, and Labangan. Table 1 lists the watersheds along with their coverage area and the included barangays. Watersheds are important in water resources for domestic supply, as they host surface water and groundwater (GW).

**Table 1.** List of Watersheds in San Jose, Occidental Mindoro [25].

Name of Watershed	Barangays Covered	Area (km <sup>2</sup> )
Busuanga	Batasan, Camburay, Central, Monteclaro, Murtha, and San Agustin	199.96
Cabariwan	Bayotbot, Labangan Poblacion, Mabini, Mangarin, Mapaya, Natandol, and Pawican	47.34
Caguray	Batasan, Bayotbot, Mapaya, Monteclaro, and Murtha	52.39
Labangan	All barangays except Mapaya	242.92

## 2.2. Sample Collection, Preparation, and Analysis

A total of 104 water samples (71 DW and 33 GW samples) were collected randomly in different barangays of the municipality of San Jose, Occidental Mindoro. The 104 grab samples were gathered using stainless steel samplers and stored in prepared acid-rinsed one liter polyethylene (PE) bottles. This is to remove the possible contaminants in the PE bottles. The PE bottles were all properly labeled, sealed, and placed temporarily in coolers. The collection, preparation, and storage of the DW and GW samples were in accordance with the EPA No. SESDPROC-301-R3 [26]. The coordinates of every sampling site were recorded utilizing a Garmin Montana 680 GPS. The sampling locations for the DW and GW are presented in Figure 2. The coordinates and corresponding elevations of the sampling locations are enumerated in Appendix B.

**Figure 2.** Sampling locations for domestic water and groundwater.

The water samples were transferred from PE bottles into zipper plastic #2 prior to detection and analysis using Olympus Vanta XRF Spectrometer and Accusensing MAS G1. High performance in situ elemental analyzers, such as the Olympus Vanta portable XRF (pXRF) and Accusensing MAS, are suitable for a variety of environmental media, including water samples. Prior to analysis, the pXRF was calibrated utilizing Olympus Vanta blank in zipper plastic #2. The XRF was set to Geochem mode. The reliability and viability on the use of Olympus Vanta XRF and Accusensing MAS for the detection of MMs in water have been discussed in various works [27–32]. The Accusensing MAS G1 was used to analyze MMs that had returned LOD readings in the pXRF [30]. Several metals and metalloid including As, Ba, Cu, Cr, Fe, Pb, Mn, Ni, and Zn were detected and used in the computation of PI and HR indices.

### 2.3. Pollution Evaluation Indices

#### 2.3.1. Metals Pollution Index (MPI)

The *MPI* can be described as the aggregate extent of the effects of MMs water resources considering human consumption and metal contamination [33,34]. The recommended standard values of the MMs was sourced out from the PNSDW 2017. The *MPI* is based on the weighted arithmetic quality mean method expressed in Equation (1).

$$MPI = \frac{\sum_{i=1}^n Q_i W_i}{\sum_{i=1}^n W_i} \quad (1)$$

$W_i$  is the weight unit and was calculated as  $1/S_i$ , wherein  $S_i$  is the recommended standard of the MMs,  $n$  is the number of estimated metals, and  $Q_i$  is the individual quality rating of the MMs, and can be calculated as expressed in Equation (2) [35].

$$Q_i = \frac{C_i}{S_i} \times 100 \quad (2)$$

wherein  $C_i$  is the measured concentration value of the MMs. The interpretation of the calculated *MPI* values were divided into three categories, such as low ( $MPI < 90$ ), medium ( $90 \leq MPI \leq 180$ ), and high ( $MPI > 180$ ) [30].

#### 2.3.2. Ecological Risk Index (ERI)

The potential *ERI* of the examined MMs was calculated by taking into account the pollution index and  $T_i$ . The *ERI* is the summation of the product of the  $T_i$  of the MMs, and the pollution index is the ratio between the concentration of the MMs in the sample and the subsequent background values. The *ERI* for each water sample was calculated using Equations (3) and (4).

$$ERI = \sum RI = \sum T_i (P_i) \quad (3)$$

$$PI = \frac{C_s}{C_b} \quad (4)$$

where *ERI* is the potential ecological risk factor of each metal,  $T_i$  is the toxic-response factor of the metal, *PI* is the pollution index,  $C_s$  is the concentration of the metals in the sample, and  $C_b$  is the corresponding background value. The toxic-response factor of the metals was as follows: As = 10, Cu = 5, Cr = 1, Fe = 1, Mn = 1, Ni = 1, Pb = 5, and Zn = 1. The interpretations of the *ERI* values were categorized as follows: low ( $ERI < 95$ ), moderate ( $95 \leq ERI < 190$ ), considerable ( $190 \leq ERI < 380$ ), and very high ( $ERI \geq 380$ ) [36,37].

#### 2.3.3. Nemerow's Pollution Index (NPI)

Based on the single factor pollution index, the *NPI* is an extensive pollution index assessment. It is applied to evaluate the WQ at various sampling locations while also emphasizing the significance of different metals concentration in the water resources. The *NPI* was calculated as the square root of the half of the sum of the squares of average and maximum single factor pollution index (SFPI), shown as Equation (5).

$$NPI = \sqrt{\frac{(SFPI_{\max})^2 + (SFPI_{\text{ave}})^2}{2}} \quad (5)$$

The SFPI is the ratio between the observed concentration and the evaluation standard of the MMs, shown as Equation (6).

$$SFPI = \frac{C_i}{S_i} \quad (6)$$

The *NPI* is divided into five classes, which includes Class 1–Unpolluted ( $NPI < 1.0$ ), Class 2–Slightly Polluted Water ( $1.0 \leq NPI < 2.5$ ), Class 3–Moderately Polluted Water ( $2.5 \leq NPI < 7.0$ ), and Class 4–Heavily Polluted Water ( $NPI \geq 7.0$ ) [37–39].

#### 2.3.4. Probabilistic Health Risk Assessment

The non–carcinogenic risk linked with oral pathway exposure to MMs, which is the hazard index (HI) shown as Equation (7), was determined by employing the summation of the *HQ* shown as Equation (8). This is the ratio between the *CDI* and *RfD*. The *CDI* was calculated using the MMs concentration, and *EF*, *ED*, *IR*, *AT*, and *BW* as shown in Equation (9) [40].

$$HI = \sum HQ \quad (7)$$

$$HQ = \frac{CDI}{RfD} \quad (8)$$

$$CDI = \frac{MC \times EF \times ED \times IR}{AT \times BW} \quad (9)$$

where *HQ* is the hazard quotient, *CDI* is the chronic daily intake, *RfD* is the reference dose, *MC* is the metal concentration, *EF* is the exposure frequency, *ED* is the exposure duration, *IR* is the ingestion rate, *AT* is the average time, and *BW* is the body weight.

The following values were utilized in the calculation: *EF* = 365 days [41], *ED* = 70 years [42], *IR* = 2 L/day [43], *AT* = 25,550 days [44], and *BW* = 70 kg [45]. The *RfD* values for each MMs (in mg/kg/day) were: As =  $3 \times 10^{-4}$  [46], Ba =  $2 \times 10^{-1}$  [47], Cu = 0.04 [5], Cr = 0.003 [48], Fe =  $7 \times 10^{-1}$  [49], Pb =  $3.5 \times 10^{-3}$  [48], Mn =  $1.4 \times 10^{-1}$  [49], Ni = 0.02 [5], and Zn = 0.3 [5].

The excess lifetime carcinogenic risk (*ELCR*) approach was utilized to calculate the risk assessment of the carcinogenicity of MMs, which utilized the product of the *SF* and the *CDI* [43]. The *SF* values employed were As = 1.5 [46], Cr = 0.5 [48], Pb =  $8.5 \times 10^{-3}$  [5], and Ni =  $8.4 \times 10^{-1}$  [5]. The *ELCR* was calculated using Equation (10) [43].

$$ELCR = CDI \times SF \quad (10)$$

#### 2.4. Spatial Mapping using Machine Learning Geostatistical Interpolation (MLGI) Approach

Utilizing the MMs concentrations detected from the water samples and their corresponding PI and MPI, spatial maps were generated by employing the MLGI method that utilized the NN-PSO algorithm and integrating it to an EBK interpolation technique. The MLGI method is the integration of a hybrid artificial neural network (ANN)–particle swarm optimization (PSO) model to the empirical Bayesian kriging method to map the MMs' concentration and pollution indices. The connection weights of the neural network models for the concentrations and pollution indices were optimized using the PSO approach, utilizing MATLAB2021a. The Levenberg–Marquardt algorithm was utilized in the algorithm training for ANN-PSO models, since it is the fastest method for moderately sized networks [38], such as used in this study. The transfer function employed was the hyperbolic tangent sigmoid function [50]. The number of iterations for the model development was 2000 iterations [51]. Figure 3 presents the chart of the process for the MLGI approach employed in this study.

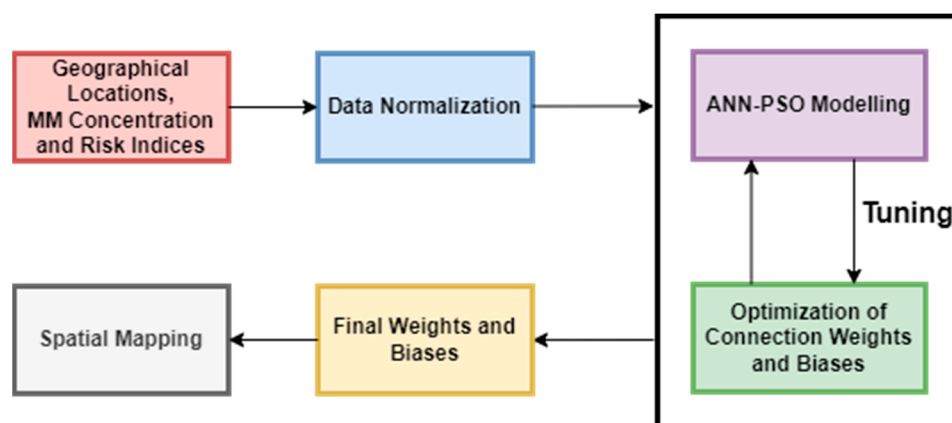


**Figure 3.** The MLGI approach employed in the study.

The spatial maps produced provided a cleared view of the state of MMs pollution in the research area, together with the associated risk it posed to the area [30].

### 2.5. Contamination Area Calculation

Using the generated spatial concentration maps by the MLGI approach, the contamination area for each MM and associated risk indices were calculated. Using the reclassification and raster to polygon conversion tool in GIS, the contamination area was calculated in reference to the reference guidelines and index reference values.

### 2.6. Statistical Analysis

Descriptive statistics were accomplished employing the Microsoft Excel Data Analysis Tool, MATLAB R2021a, and R Studio software. The evaluation for the normality of data were evaluated employing the Shapiro-Wilk test for GW (less than 50 samples) and the Kolmogorov-Smirnov test for DW samples (greater than 50 samples) [49]. Moreover, the variability of the GW and DW samples was analyzed using the coefficient of variability (CV), wherein CV less than or equal to 15% is low; CV greater than 15% but less than or equal to 35% is intermediate; and CV greater than 35% is high [26]. Furthermore, the mean concentration was compared to the PNSDW 2017 standard values.

The MMs concentrations correlations of water samples were analyzed using a multivariate Pearson correlation matrix. In order to demonstrate the correlation concerning the investigated parameters, particularly with regard to their sources, Pearson's correlation analysis was performed on the data using MATLAB R2021a and R Studio software [52]. Parameters with a correlation coefficient of  $0.90 \leq R \leq 1.00$  indicate a very strong correlation;  $0.70 \leq R \leq 0.89$  suggests a strong correlation;  $0.40 \leq R \leq 0.69$  denotes a moderate correlation;  $0.10 \leq R \leq 0.39$  signifies a weak correlation; and  $0.00 \leq R \leq 0.09$  indicates a negligible correlation [53]. Additionally, pairings with strong and moderate coefficients suggest considerable risk factors, whereas those with weak coefficients suggest low risk factors [54].

## 3. Results and Discussion

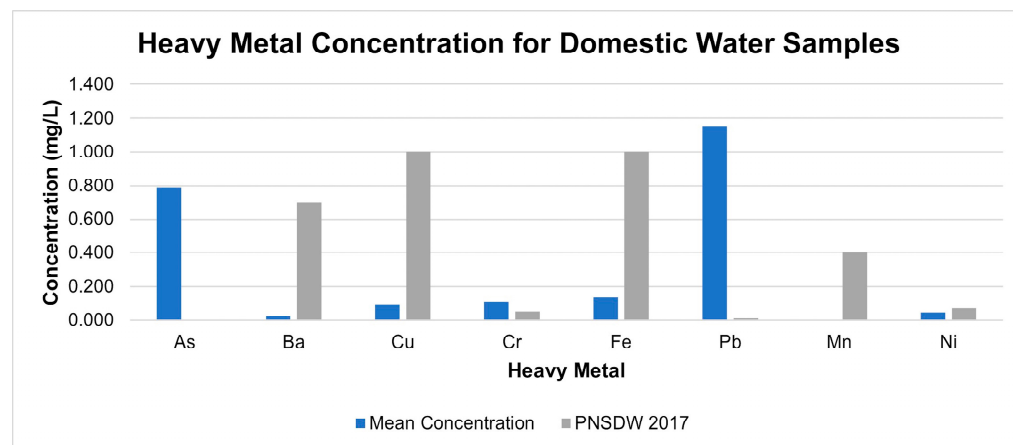
### 3.1. Metal Concentration

The basic statistical parameters of the MMs in DW samples from various locations in San Jose, Occidental Mindoro are presented in Table 2. The trend of MMs' mean concentration detected in DW was  $Pb > As > Fe > Cr > Cu > Ni > Ba > Mn$ . The Kolmogorov-Smirnov test showed that the MMs concentration in DW in the research area was not uniformly distributed, since all the metals have  $p < 0.05$  [55]. Moreover, the CV values for all the detected MMs exhibited values higher than 35%. This suggests that the acquired datasets for the DW samples have high variability.

**Table 2.** Metals and metalloid concentrations (in mg/L) in DW.

	As	Ba	Cu	Cr	Fe	Pb	Mn	Ni
N	71.000	71.000	71.000	71.000	71.000	71.000	71.000	71.000
Max	6.680	0.050	0.800	0.890	1.820	15.160	0.020	0.720
Min	0.000	0.000	0.000	0.000	0.000	0.000	0.000	0.000
Mean	0.792	0.024	0.093	0.110	0.138	1.152	0.003	0.045
SD	1.762	0.016	0.157	0.225	0.279	3.302	0.004	0.152
Skewness	2.228	−0.629	2.493	2.172	3.895	3.538	1.592	3.314
Kurtosis	3.716	−1.107	7.019	3.878	19.340	12.349	2.552	9.867
CV%	222.640	66.560	168.250	205.150	202.610	286.580	137.570	339.760
PNSDW	0.010	0.700	1.000	0.050	1.000	0.010	0.400	0.070

The mean concentrations of the MMs were compared to the PNSDW 2017 as shown in Figure 4. The DW dataset obtained revealed that As, Cr, and Pb were above the threshold standards set by the PNSDW 2017 by 79.2, 2.2, and 115.2 times, respectively. About 33.8% of the sampling site was above the PNSDW 2017 threshold limit for As, while that for Cr, Fe, Pb, and Ni were 26.8%, 2.8%, 31%, and 8.5%, respectively. Additionally, all sampling sites for Ba, Cu, and Mn were under the PNSDW 2017 standard limits.

**Figure 4.** Comparison of MMs' concentrations in DW with PNSDW 2017 standard values.

The highest Fe concentration in DW was 1.8 times greater than the standard value and was detected in a deep well water source in Brgy. Iling Proper. Elevated Fe concentration may lead to Fe poisoning. Localized iron poisoning is characterized by gastrointestinal bleeding, nausea, vomiting, and abdominal discomfort. Injuries to the liver and cardiovascular system lead to systemic toxicity [56]. For the detected Ni concentration in DW samples, the highest detected concentrations were recorded in Barangay II Poblacion. The water samples were collected from a water refilling station (WFS) with a concentrations 10.3 times greater than the standard limit set by PNSDW. Exposure to elevated Ni concentration can have neurological side effects such as giddiness, fatigue, and headaches. The effects of drinking nickel-tainted water on the gastrointestinal system includes nausea, cramping in the abdomen, diarrhea, and vomiting. Additionally, impacts on the musculoskeletal system, including muscular discomfort, have been linked to drinking nickel-contaminated water [57].

Moreover, the highest concentrations of Pb was detected in Brgy. Camburay, collected from a WRS with concentrations of 1516 times greater than the PNSDW limit. The Pb exposure has many hazardous consequences, but might be reversed if discovered promptly. However, chronic high-level Pb exposure has the potential to permanently harm the kidneys, central nervous system, and peripheral nervous system [58]. Acute lead poisoning can cause a number of different signs and symptoms, such as abdominal discomfort, constipation, joint pain, muscular aches, headaches, anorexia, reduced libido,

difficulties focusing and short-term memory deficiencies, irritability, excessive tiredness, sleep disturbances, and anemia [59,60].

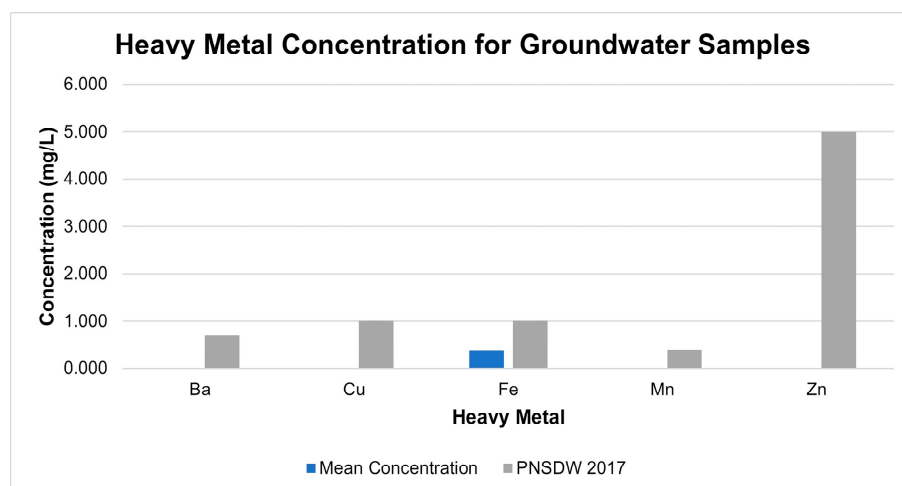
Highest Cu concentrations were detected in 3 different locations. These are Brgy. Iling Proper, Brgy. Ipil, and Brgy. Murtha. The highest concentrations of Mn and Zn were recorded in Brgy. Central and Brgy. San Agustin, respectively. However, the concentration levels of Cu, Mn, and Zn detected were inside the PNSDW 2017 limit. The highest Ba levels in GW were observed in Brgy. Batasan, and the detected concentration was 2.15 times greater than the PNSDW 2017 limit.

Table 3 exhibits the descriptive statistics of the GW samples in the research area. The trend of mean concentrations for the GW samples was  $Fe > Zn > Ba > Mn > Cu$ . The Shapiro-Wilk test revealed that the data array for the GW samples were not normally distributed with  $p < 0.05$  [61]. Additionally, all the CV values were greater than 35%, which indicates that the data variability is high.

The mean concentrations for GW samples were compared to the PNSDW 2017, as shown in Figure 5. All mean concentrations of the GW samples were below the threshold values set by the PNSDW 2017. Among the MMs detected in the GW samples, only the Fe concentration was recorded above the PNSDW 2017 standard values in various sampling locations.

**Table 3.** Metal and metalloid concentrations (in mg/L) in GW.

	Ba	Cu	Fe	Mn	Zn
N	33	33	33	33	33
Max	0.020	0.010	5.700	0.020	0.050
Min	0.000	0.000	0.000	0.000	0.000
Mean	0.0051	0.0007	0.3716	0.0047	0.0056
SD	0.006	0.002	1.213	0.005	0.012
Skewness	1.209	2.868	3.897	0.995	2.207
Kurtosis	1.149	6.654	14.832	0.455	4.511
CV%	114.31	310.56	326.63	102.27	220.23
PNSDW	0.700	1.000	1.000	0.400	5.000



**Figure 5.** Comparison of MM concentrations and PNSDW 2017 threshold values for groundwater samples.

The extent of the relationship between the MMs in water samples was determined using the Pearson correlation. The correlation plots for the (a) DW and (b) GW samples are presented in Figure 6. Findings demonstrated that a positive correlation was shown between Cr and Cu in DW samples. Similar findings were observed in water quality studies in Saudi Arabia [62], India [63], Sri Lanka [64], Egypt [65], Burkina Faso [66], Greece [67], Iran [68], and Turkey [69]. Likewise, a positive correlation between Fe and Zn was

observed and comparable to the result of the studies by Atangana and Oberholster [70], Esmaeili et al. [71], Duggal et al. [72], Varghese and Jaya [73], and Karthikeyan et al. [74]. The correlation analysis that was conducted revealed a positive association between Cr and Cu and Fe and Zn. This is attributed to a potential common origin of these MMs and could be the controlling factor of the MMs' concentration in the water resources [75]. The findings of the study are an evidence of the potential contamination of water resources and/or water supplies lines and present a direction of necessary treatment strategy. These findings should be utilized to create and develop remediation programs to mitigate the effects of these MMs in the community.

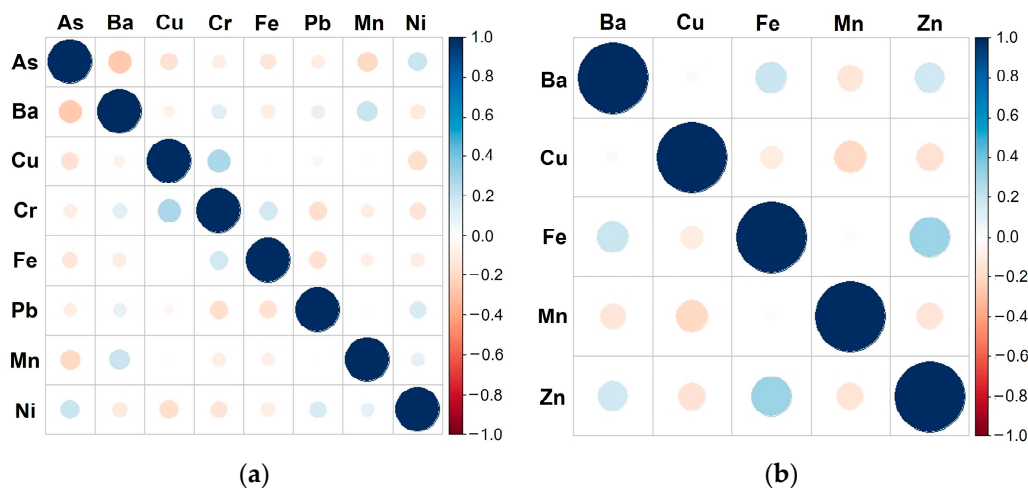


**Figure 6.** Correlation plots for metals and metalloid in (a) DW; and (b) GW samples.

### 3.2. Pollution Evaluation Indices

Using the MMs' concentrations detected in the water samples, the *MPI*, *NPI*, and *ERI* were calculated. The mean *MPI* value calculated in DW samples was 90 times greater than the upper limit of the "low" pollution *MPI* category, while the sampling point observed with the highest *MPI* value was 701 times larger. Considering the GW, the mean *MPI* value was below the upper boundary of the "low" pollution category. The mean *NPI* values for DW revealed that the average calculated *NPI* values were 135 times greater than the upper threshold for the unpolluted location criterion. Moreover, the highest *NPI* calculated was 1080 times the unpolluted threshold limit. On the other hand, the GW mean *NPI* values were within the unpolluted category. The mean *ERI* value calculated for DW was 3.5 times the upper limit of the "low" *ERI* category, while that of the highest *ERI* observed was 23.8 times larger. For the GW samples, the mean *ERI* value calculated was within the "low" *ERI* category.

### 3.3. Probabilistic HRA

The mean *HQ* with regards to the MMs was calculated from DW samples. It was found out that the *HQ* for As, Cr, and Pb have mean *HQ* values greater than 1. This suggests that potential non-carcinogenic consequences may arise [76]. The mean *HI* for the DW samples was 86 times larger than the limit, which indicates that there is a greater possibility of harmful consequences [77]. The trend of the mean *HQ* values in DW samples was  $As > Pb > Cr > Cu > Ni > Fe > Ba > Mn$ , wherein As can be attributed to 88% of the mean *HQ* value.

The mean *HQ* values in GW samples for Ba, Cu, Fe, Mn, and Zn were below 1. Moreover, the mean *HI* value was also less than 1. This means that there was non-carcinogenic risk for Ba, Cu, Fe, Mn, and Zn in GW. The highest mean *HQ* observed was for Fe, but the calculated value was still below 1. The trend of the mean *HQ* values in GW samples was  $Fe > Mn > Ba > Zn > Cu$ . The concentration of Fe contributes to the 85% of the mean *HQ*

value. The contribution of each MM to the *HQ* is shown in Figure 7a,b. It was observed that *HQ* for As was the significant contributor to the total *HI* value.

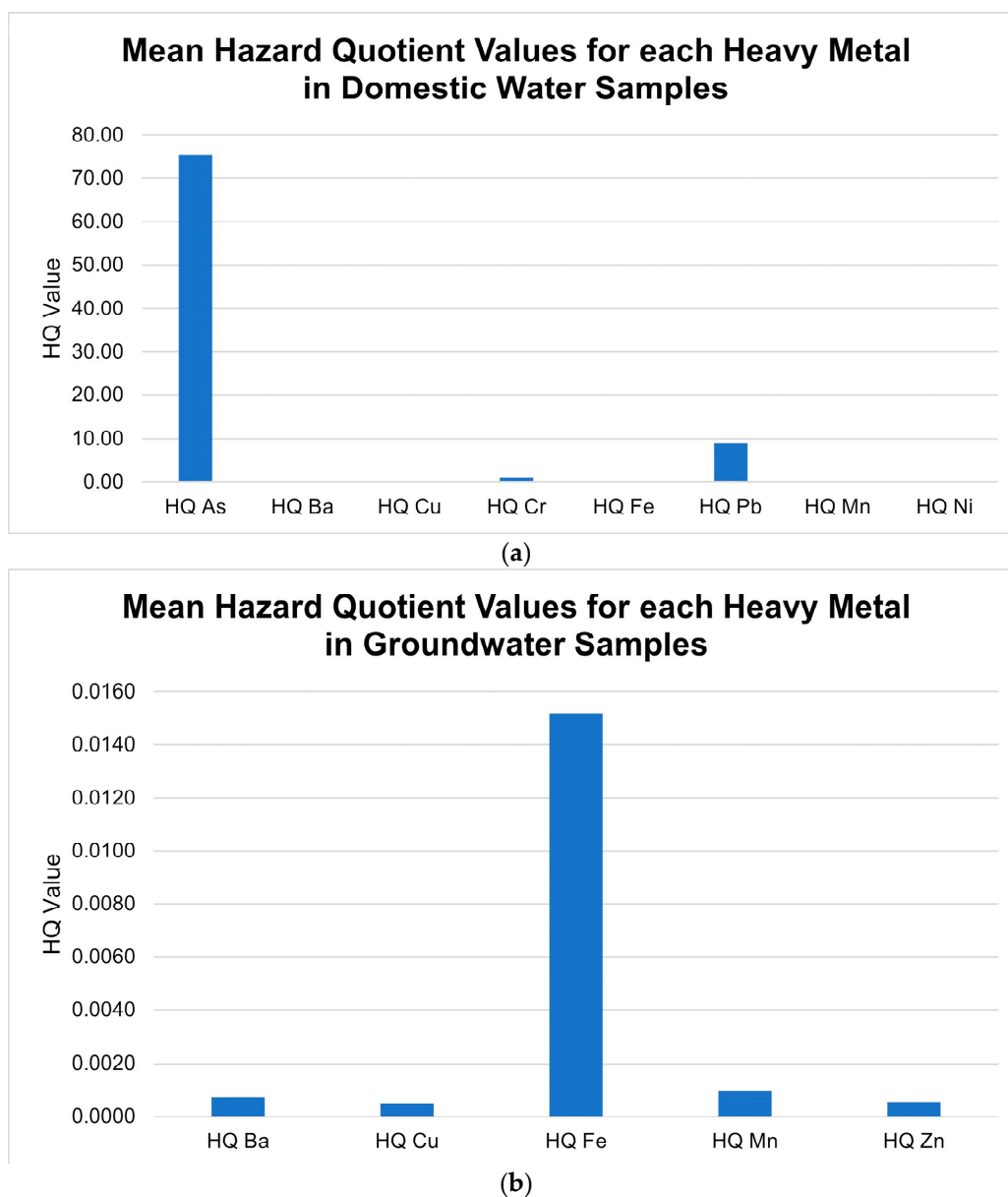


**Figure 7.** Mean HQ values for each MM in (a) DW; and (b) GW samples.

The *ELCR* was only calculated for DW samples, since the metal concentrations of As, Cr, Pb, and Ni were not detected in GW samples. The trend of the *CR* values observed in DW was  $As > Cr > Ni > Pb$ . The As concentration contributed to the 92.06% of the *ELCR* value.

The summary of the number of sampling locations exceeding the *HQ* threshold limit is presented in Figure 8. About 33.8% of DW sampling sites had the *HQ* value of As above the threshold, while that of Cr, Pb, and Ni were 23.9%, 28.2%, and 1.4%, respectively. No sampling point recorded an *HQ* value above the threshold value for GW sampling sites.

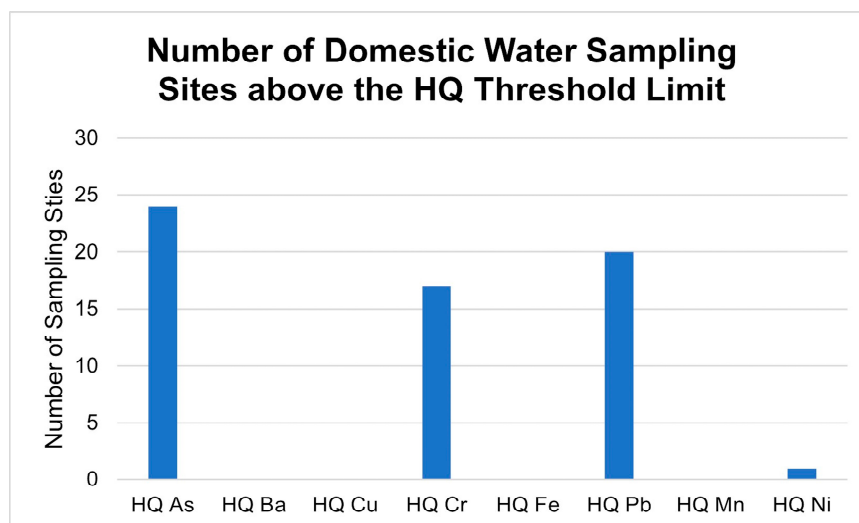


**Figure 8.** Number of DW sampling sites above the HQ threshold limit.

Considering the *ELCR* values, the summary of the number of sampling sites categorized to have medium to very high cancer risk is shown in Figure 9. About 35.2% of the sampling sites for DW had CR categorized as “medium to very high cancer risk”. Additionally, Cr, Pb, and Ni were 26.8%, 29.6%, and 8.5%, respectively, and categorized as ‘medium to very high cancer risk’.

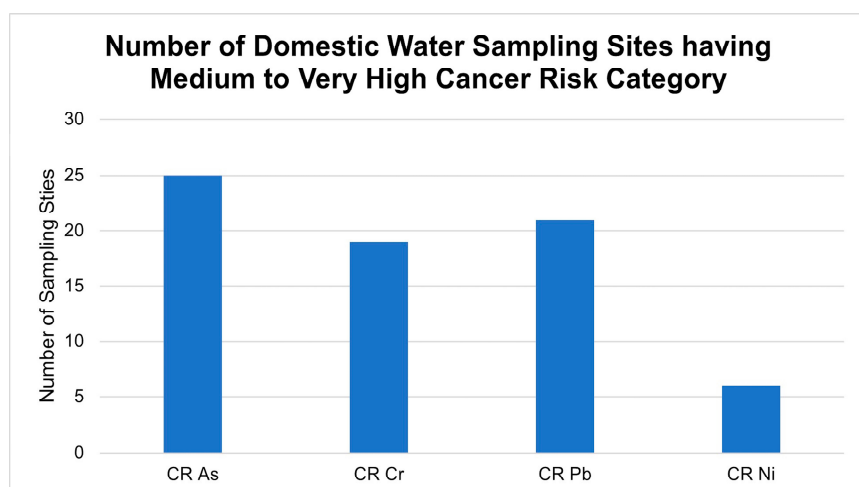


**Figure 9.** Number of DW sampling sites categorized to have medium to very high cancer risk.

### 3.4. Spatial Mapping using MLGI Approach

Spatial maps were produced using the MLGI technique, which combines NN-PSO using the MM concentrations observed in the water samples and their link with PI and HR indices. Table 4 summarizes the results of the simulation for the MLGI mapping of the MMs in DW samples using the hybrid NN-PSO+EBK approach. Figure A1 in Appendix C presents the produced spatial maps for the MMs in DW samples.

The results of the simulation for the hybrid NN-PSO+EBK method to the MLGI mapping of the pollution indices in the DW samples are displayed in Table 5. Figure A3 in Appendix C displays the spatial maps for the pollution indices in the DW samples.

The highest concentrations for Ba in DW samples were detected in Brgy. San Agustin and Brgy. Mangarin, while the highest concentrations for Cu and Mn were detected in Brgy. Monteclaro and Brgy. San Roque. However, the highest Ba, Cu, and Mn concentrations detected were within the limit of PNSDW 2017.

**Table 4.** NN-PSO simulation results for metals and metalloid in DW samples.

	HN	NP	NI	ET (s)	Validation	Testing
As	25	9	2000	124.18818	0.98617	0.99656
Ba	29	6	2000	124.47877	0.95023	0.98621
Cr	29	3	2000	160.77287	0.96793	0.98507
Cu	30	7	2000	121.85391	0.98758	0.94860
Fe	22	7	2000	128.33642	0.95715	0.97733
Mn	25	2	2000	125.32753	0.94777	0.93157
Ni	28	7	2000	153.38283	0.99861	0.99971
Pb	29	9	2000	122.88486	0.99728	0.98994

The pollution hotspot for As in DW was observed in Brgy. Bubog, and the water samples were collected from WRS with an As concentration 668 times greater than the PNSDW 2017 standard value. Exposure to As has been associated with several health consequences such as skin and neurological diseases, cancers, and non-communicable diseases, including hypertension and diabetes mellitus [78]. The highest concentration of Cr was detected in a spring from Brgy. Labangan Iling with a concentration 17.9 times greater than the PNSDW 2017. Exposure to elevated concentrations of Cr may decrease the glycemic tolerance factor and raise the risk of cardiovascular disease [79]. Oral intake of Cr usually causes various symptoms such as stomach ulcers, nausea, vomiting, fever, vertigo, diarrhea, liver damage, and even death at doses from 1 to 3 g [80,81].

**Table 5.** NN-PSO simulation results for pollution indices in DW samples.

Index	HN	NP	NI	ET (s)	Validation	Testing
HPI	27	8	2000	128.95811	0.98384	0.99973
NPI	29	5	2000	130.91300	0.99203	0.99400
ERI	30	1	2000	140.66034	0.98862	0.98091

Table 6 shows the outcomes of the simulation for the MLGI mapping of the MMs in the GW samples utilizing the hybrid NN-PSO+EBK approach. The spatial maps for the MM in the GW samples are presented as Figure A2 in Appendix C.

**Table 6.** NN-PSO simulation results for metals and metalloid in GW samples.

	HN	NP	NI	ET (s)	Validation	Testing
Ba	25	6	2000	125.76638	0.92786	0.97901
Cu	27	7	2000	132.61975	0.99957	0.99987
Fe	30	2	2000	141.61058	0.99868	0.99706
Mn	29	3	2000	143.39959	0.99152	0.99922
Zn	26	1	2000	150.94246	0.99997	0.99994

Ingestion is one the mechanisms that allow Ba to enter the human body [82]. Acute toxicity of Ba consists of gastrointestinal, metabolic, cardiovascular, musculoskeletal, and neurological effects. Gastrointestinal effects include gastric pain, nausea, vomiting, and diarrhea [83]; metabolic effects include hypokalemia, ventricular tachycardia, and hypertension or hypotension [84]; cardiovascular effects include changes in the heart rhythm and increased or decreased blood pressure [85]; skeletomuscular effects include numbness, muscle weakness, and paralysis [86]; and neurological effects including tremors, seizures, and mydriasis. Another, the hotspot area for Fe was detected in a deep well in Brgy. Bubog, which is 5.7 times greater than the PNSDW threshold. It should be noted that Fe poisoning is frequently fatal due to shock or liver failure [87].

Considering the measure of the cumulative impact of MMs on DW resources, with respect to the human consumption and metal pollution, the *MPI* hotspot was observed in Brgy. Camburay. The DW quality at various sampling locations, with the emphasis on the importance of different MMs in the water resources, was measured using the *NPI*. The highest *NPI* was likewise observed in Brgy. Camburay. Moreover, the highest *ERI* values were observed in a residential DW source in Brgy. Bubog.

Table 7 displays the outcomes of the simulation for the hybrid NN-PSO+EBK approach to the MLGI mapping of the pollution indices in the samples of GW. The spatial maps for the pollution indices in the GW samples are displayed in Figure A4 in Appendix C.

**Table 7.** NN-PSO simulation results for PI in GW samples.

Index	HN	NP	NI	ET (s)	Validation	Testing
<i>HPI</i>	26	2	2000	149.06667	0.99962	0.99984
<i>NPI</i>	29	3	2000	141.51668	0.99869	0.99781
<i>ERI</i>	28	4	2000	142.93539	0.98216	0.99958

The *HPI*, *NPI*, and *ERI* hotspots were found in a deep well at Brgy. Bubog. The simulation results for the MLGI mapping of the *HQ/HI* values in the DW samples are demonstrated in Table 8. Figure A5 in Appendix C displays the spatial maps for the pollution indices in the GW samples.

**Table 8.** NN-PSO simulation results for hazard quotient/hazard index in DW samples.

Index	HN	NP	NI	ET (s)	Validation	Testing
<i>HQ (As)</i>	29	5	2000	131.72678	0.98983	0.99024
<i>HQ (Ba)</i>	27	2	2000	119.00130	0.96164	0.93469
<i>HQ (Cr)</i>	29	5	2000	114.47954	0.98674	0.98510
<i>HQ (Cu)</i>	28	7	2000	116.09329	0.99268	0.99534
<i>HQ (Fe)</i>	26	7	2000	114.40573	0.99709	0.99748
<i>HQ (Mn)</i>	29	9	2000	115.17782	0.98861	0.99820
<i>HQ (Ni)</i>	26	7	2000	121.11026	0.97369	0.94806
<i>HQ (Pb)</i>	27	8	2000	126.85262	0.98794	0.96551
<i>HI</i>	28	2	2000	118.55610	0.98692	0.98708

The calculated *HQ* for Ba, Cu, Fe, and Mn was observed to be less than 1 for DW samples. The highest *HQ* for As was observed in Brgy. Bubog, which is 637 times greater than the recommended *HQ* of less than 1. The *HQ* of Cr was observed in Brgy. Labangan Iling from a spring. It was observed to be 8.5 times higher than the recommended *HQ* value. The *HQ* for Ni was 1.03 times higher than suggested *HQ* value and was detected in Barangay II Poblacion, and was collected in a WRS. The *HQ* for Pb was 120.3 times higher than the recommended *HQ* value and was observed in Brgy. Camburay, also collected from WRS. Moreover, the *HI* for DW was calculated to be 647 times above the standard value. This was observed in Brgy. Bubog, collected from WRS.

Table 9 displays the simulation results for the MLGI mapping of the GW samples' *HQ/HI* values. The spatial maps for the pollution indices in the GW samples are presented as Figure A6 in Appendix C.

The *HQ* observed in GW samples for Ba, Cu, Fe, Mn, and Zn were all lower than the recommended *HQ* value of 1. Consequently, the overall *HI* in all sampling locations was below 1, which suggests that there is non-carcinogenic risk of exposure to Ba, Cu, Fe, Mn, and Zn in GW.

The MLGI mapping of the simulation results for the carcinogenic risk (*CR*) index values of DW samples is shown in Table 10. Figure A7 Appendix C shows the spatial maps

for the CR values by As, Cr, Pb, Ni, and the total carcinogenic risk evaluation in the GW samples.

**Table 9.** NN-PSO simulation results for HW/HI in GW samples.

Index	HN	NP	NI	ET (s)	Validation	Testing
HQ (Ba)	26	7	2000	137.11112	0.99029	0.97838
HQ (Cu)	27	10	2000	136.08892	0.99998	0.99997
HQ (Fe)	28	10	2000	123.77389	0.99662	0.99922
HQ (Mn)	27	3	2000	134.97920	0.99599	0.99213
HQ (Zn)	29	5	2000	132.29242	0.99781	0.99719
HI	26	9	2000	135.89116	0.99918	0.99589

**Table 10.** NN-PSO simulation results for CR index in DW samples.

Index	HN	NP	NI	ET (s)	Validation	Testing
CR (As)	27	5	2000	139.80123	0.98699	0.99963
CR (Cr)	23	1	2000	139.84580	0.99420	0.99058
CR (Pb)	30	6	2000	131.91650	0.99112	0.99518
CR (Ni)	28	9	2000	179.67048	0.97320	0.97238
TCR	26	4	2000	138.49763	0.99742	0.99289

The hotspot for the CR with respect to As and Ni concentrations was observed in Barangay Población II. The highest CR for Cr concentration was observed in Brgy. Labangan Iling. The CR for Pb was recorded at Brgy. Camburay. All these highest CRs observed were considered to have a very high CR. The mean CR index levels for As, Cr, and Ni in the study area were classified to have a very high CR, while that for the CR of Pb was considered to have a high carcinogenic risk.

### 3.5. Contamination Area Calculation

Pollution indexes such as *MPI*, *NPI*, and *ERI* were calculated to establish the effect of the group of MMs in the DW and GW resources of San Jose, Occidental Mindoro. Considering the DW in the research area, the hotspots for *MPI* and *NPI* were observed in Brgy. Camburay, which inhabited by about 1900 people. On the other hand, Brgy. Bubog was observed to be the *ERI* hotspot, considering the DW and GW in the research area. It is also the hotspot for *MPI* and *NPI* with reference to the groundwater resources in the research area. Brgy. Bubog has a population of about 10,800 people, comprising about 7% of the total population of the municipality of San Jose.

Using the generated spatial maps of MMs and their associated risk index values, the contamination area was calculated using the reclassification and raster to polygon tools of ArcGIS 10.8.1. The contamination area percentages, considering the MMs in DW and GW samples, were shown in Figure 10. It was observed that 100% of DW samples in the entire study area were below the PNSDW 2017 limit for Ba, Cu, and Mn. The % area affected by Cr, Fe, and Ni was 19.9%, 4.2%, and 16.0%, respectively. Moreover, 51.1% and 72.7% of the DW samples in the study area were contaminated with As and Pb, respectively. Considering the MMs' contamination % area in GW, 100% of the total area was below the PNSDW 2017 limit for Ba, Cu, and Mn. However, Fe and Zn affected only 4.1% of the total study area.

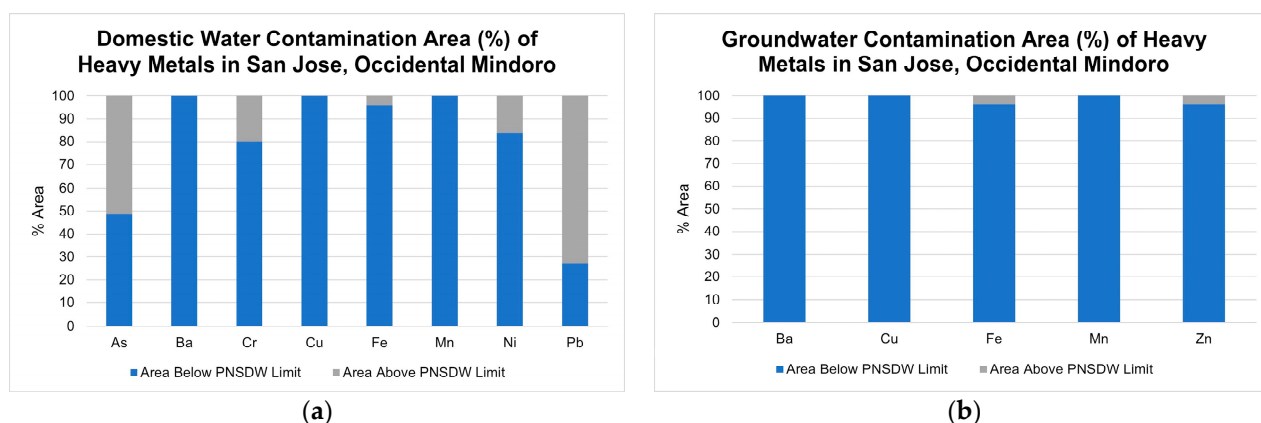


**Figure 10.** Contamination area (%) of MMs calculated for (a) domestic water; and (b) groundwater.

The contamination area percentages, considering the pollution risk indices, including *MPI*, *NPI*, and *ERI* in DW and GW samples, are shown in Figure 11a–c. Considering the *MPI* in DW, 38.7% of the study area was classified to have a high *MPI*, while the GW is recorded as 0.6%. This “high” *MPI* classification suggests that DW quality in San Jose, Occidental Mindoro is unsuitable as DW. About 96.0% and 3.4% of the DW and GW, respectively, recorded an *NPI* of “moderately to heavily polluted”. Moreover, 100% of the GW samples were classified to have “low to moderate” *ERI*, while 30.0% of the area of DW was classified to have “considerable to very high” *ERI*.

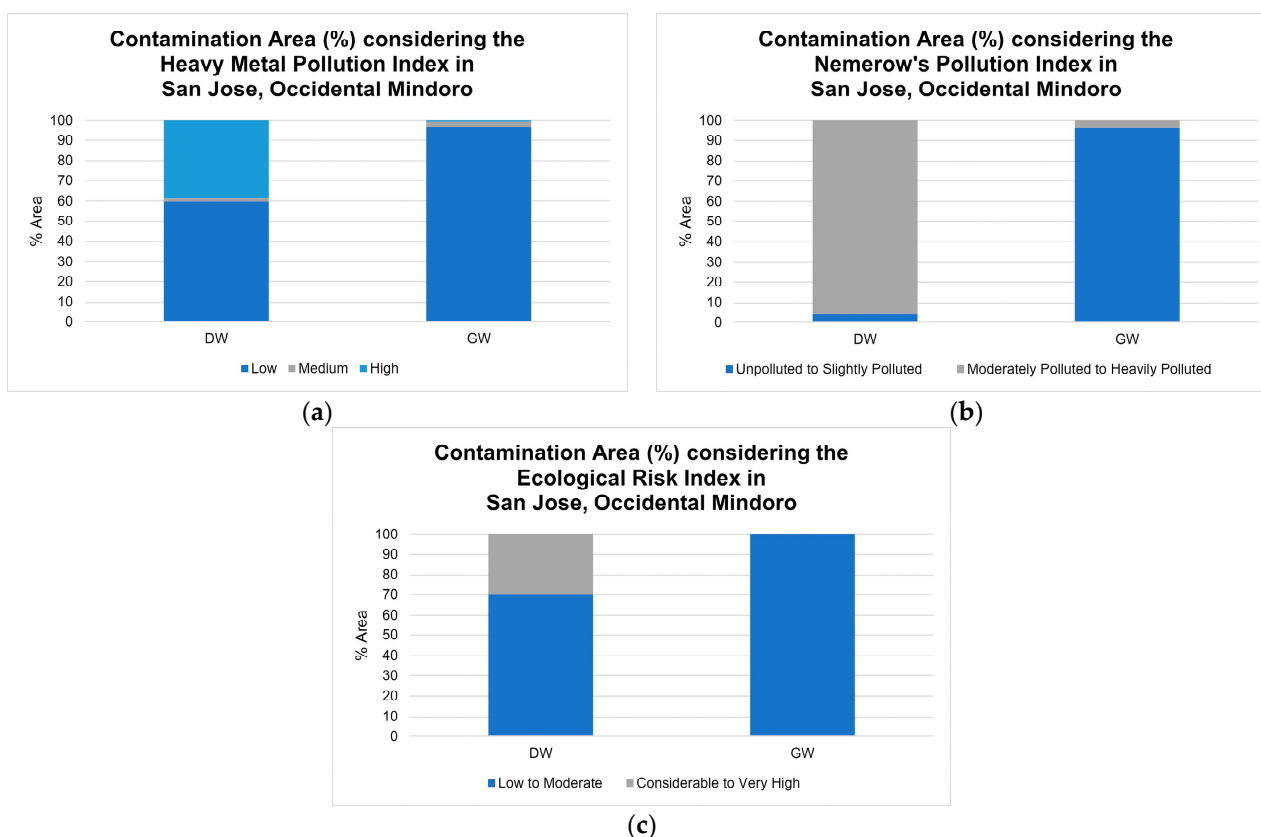


**Figure 11.** Contamination area (%) calculated for (a) *HPI*; (b) *NPI*; and (c) *ERI* in domestic water and groundwater.

The contamination area percentage, considering the HW in DW and GW, is shown in Figure 12a,b. It was observed that 100% of DW in the study area has an *HQ* value less

than 1 for Ba, Cu, Fe, and Mn. More than 60% of the study area has an *HQ* value greater than 1 with respect to Cr and Pb. Moreover, there was no area with *HQ* greater than 1 in the GW samples as shown in Figure 12b with no color gray.

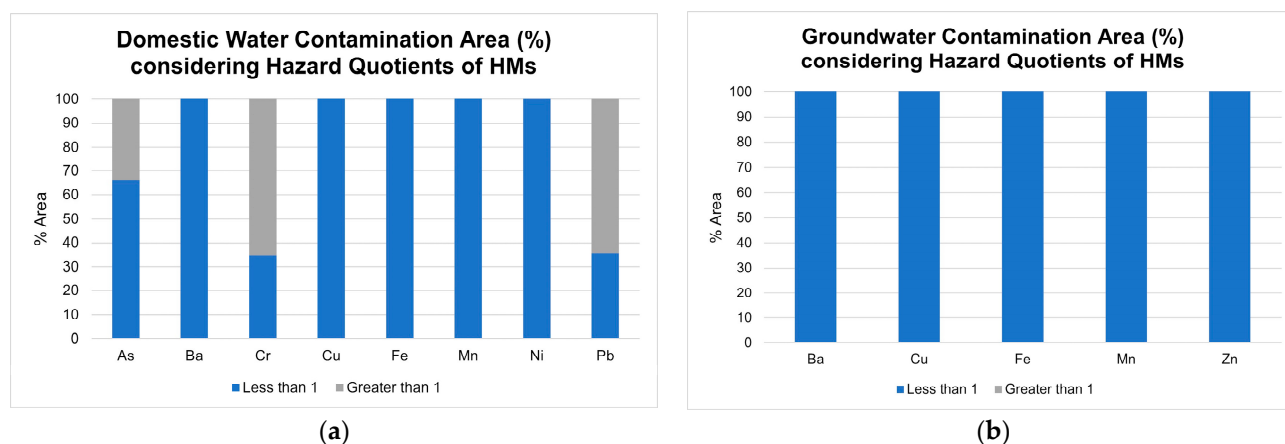


**Figure 12.** Contamination area (%) of *HQ/HI* in MMs calculated for (a) domestic water; and (b) groundwater.

Figure 13 presents the area percentage of the GW and DW that was contaminated when the total carcinogenic risk (*TCR*) was taken into account. The calculation showed that 93.3% of the area was classified as “high to very high” *TCR*. This implies that there is potential carcinogenic risk in the population due to oral exposure of carcinogens from DW supply.

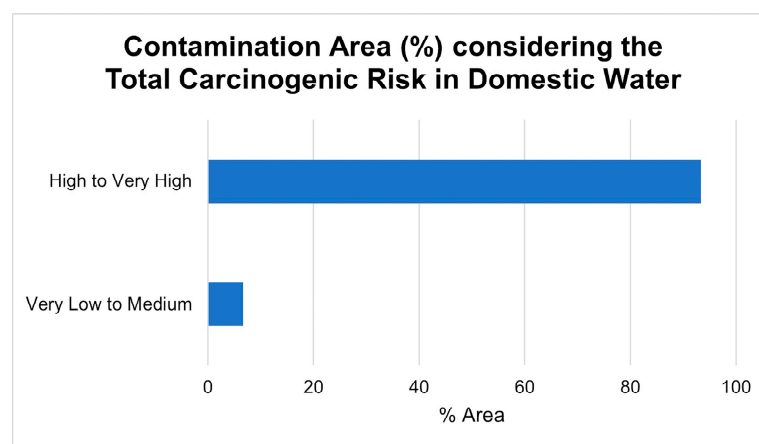


**Figure 13.** Contamination area (%) of *TCR* in domestic water.

The trend of MMs were noted as  $Pb > As > Fe > Cr > Cu > Ni > Ba > Mn$ , while the trend for GW was  $Fe > Zn > Ba > Mn > Cu$ .

Results of the correlation analysis showed that Cr and Cu in DW samples had a positive correlation. This was attributed to the eroding of igneous rocks in the region [88,89]. Moreover, Fe and Zn were positively correlated, which implies that the MMs appear to have a geogenic origin [90].

The carcinogenicity of MMs concentration was caused primarily by ingestion [88] and the dose. The *HQ* levels greater than 1 indicate high potential health risks [87]. The *HQ* for As contributed to 87.9% of the hazard index in DW, while Pb and Cr contributed to 10.7% and 1.2%, respectively. The rest of the *HQs* for Ba, Cu, Fe, Mn, and Ni were less than 1%. The *HQ* for GW resources in reference to Ba, Cu, Fe, Mn, and Zn were all less than 1. The carcinogenic risk was calculated for domestic water and was observed to have a trend of  $As > Cr > Ni > Pb$ . This implies that the *CR* for As was significantly more elevated

than Cr, Ni, and Pb, and was the main carcinogenic MMs area. Considering the calculated *TCR* in the study area, 40 of 71 sites were classified to have a “high” and “very high” cancer risk category.

Based on these results, several sites, including Brgy. Poblacion II, Brgy. Labangan Iling, and Brgy. Camburay, were considered pollution hotspots and have become the priority sites for remediation. Also, it is necessary to conduct regular DW quality monitoring with respect to MMs in the area. Updating of relevant local and national laws, policies, and guidelines becomes necessary. The knowledge of the community of the hazards posed by the MMs through water resources shall be continuously enhanced to reduce the risks and adverse health effects. Therefore, installing and using appropriate water treatment will be beneficial to lessen the HR caused by the MMs content in DW [91]. A thorough assessment of the environmental quality and health cases of the population must be carried out to create more effective health risks reduction strategies and remediation approaches in the area.

It is a requirement of the Philippine government that water utility companies meet the minimum national water quality standards before distributing water to the community; however, monitoring of such should be improved to ensure that the WQ parameters, especially MMs, are within the PNSDW standards. Also, many areas in the country are not receiving water from a utility company, especially those in the far-flung areas. The people in the community typically get the water from deep wells, shallow wells, and springs and is consumed directly without treatment. According to the WHO and UNICEF, as of 2020, only 47% of the Philippines’ total population has access to safely managed drinking water services [92].

The use of machine learning techniques and algorithms as predictive models for spatial mapping has become necessary to areas, such as San Jose, Occidental Mindoro, that are remote, and regular water quality assessment and evaluation is a challenge. The application of the machine learning approach and algorithms generated a hybrid method for mapping parameters in various studies, including the use of kernel logistic regression [93], differential flow pollination [94], logistic regression, random forest [95], reduced error pruning trees [96], least squares support vector classification–bat algorithm [97], gradient-boosted trees, and support vector machine [98]. These characteristics of the MLGI become suitable to the mapping needs in this kind of condition. The current study has proven that the use of a hybrid method, the MLGI approach, to map the pollution index and health risks in the region is an efficient and reliable method for evaluating potential sources and hotspots of pollution. The study’s findings could serve as the foundation for thorough water management in the area to guarantee safe and viable water resources in the municipality and regions of similar conditions. Research and further studies that would lead to identifying the appropriate remediation technology, policies, and guidelines for regular water quality monitoring of MMs in DW, mitigation measures, and other relevant interlinked laws are necessary. Prompt action from the municipal health and sanitation offices is required.

#### 4. Conclusions

A total of 104 DW and GW samples collected from the municipality of San Juan, province of Occidental Mindoro, Philippines were analyzed for the presence of target MMs such as As, Ba, Cu, Cr, Fe, Pb, Mn, Ni, and Zn. Reliable and high-performance portable Olympus Vanta XRF and Accusensing MAS devices were used to detect and analyze the water samples for the target MMs. The detected concentrations of these MMs were compared to PNSDW 2017 limits and used in the calculation of the *MPI*, *ERI*, *NPI*, and *ELCR*. This is to determine the suitability of the water resources for domestic use and the risks posed by the elevated concentration of these MMs. Further, this study employed the use of GIS and the MLGI technique to further reinforce the calculated pollution indices to identify the pollution hotspots. Based on the recorded results, the DW samples collected had critical concentrations of MMs compared to the GW samples. The Pb concentration

recorded the highest mean among other MMs in DW, while the Fe concentration was the highest mean concentration recorded for GW. The mean *NPI* for DW was 135 times greater than the upper limit of the unpolluted location category. The highest *NPI* recorded was 1080 times higher than the upper limit of the unpolluted site category. The calculated *ERI* in the area was 23.8 times higher than the upper limit for 'low' *ERI* category. The trend of the mean MM concentrations in the DW was Pb (1.152 mg/L) > As (0.792 mg/L) > Fe (0.138 mg/L) > Cr (0.110 mg/L) > Cu (0.093 mg/L) > Ni (0.045 mg/L) > Ba (0.024 mg/L) > Mn (0.003 mg/L). Based on the calculated *MPI*, *NPI*, and *ERI*, it was observed that the pollution hotspot was noted at Brgy. Camburay and Brgy Bubog. It was recorded that 33.8% and 28.2% of San Jose Municipality had DW containing elevated concentrations of As and Pb, respectively. Also, it was observed that As was contributing significantly to the total carcinogenic health risks in the area. Using the MLGI approach, the contamination area projected by DW samples was calculated and showed that 96.0% of the study area was classified to be moderately to heavily polluted. About 35.2% of the sampling sites for DW have carcinogenic risk category of medium to very high risk specific to elevated concentrations of Cr, Pb, and Ni. The carcinogenic risk hotspots for As, Cr, Pb, and Ni were Barangays Poblacion II for As and Ni; Barangay Labangan II for Cr; and Brgy Camburay for Pb. The conduct of pollution, health risk evaluation, and the use GIS with MLGI mapping to describe the pollution indices and ecological and health risks in specific areas are effective and reliable approaches in evaluating potential pollution sources and hotspots. The extracted data are useful in creating strategic programs for health risk reduction, as well as the mitigation and remediation of polluted areas. The result of this study is useful in water resource management in the area and neighboring regions.

**Author Contributions:** Conceptualization, D.B.S. and K.L.M.D.J.; methodology, D.B.S., K.L.M.D.J. and C.E.F.M.; software, K.L.M.D.J. and C.E.F.M.; validation, D.B.S., K.L.M.D.J. and C.E.F.M.; formal analysis, K.L.M.D.J. and C.E.F.M.; investigation, D.B.S. and K.L.M.D.J.; resources, D.B.S.; data curation, D.B.S. and K.L.M.D.J.; writing—original draft preparation, K.L.M.D.J. and C.E.F.M.; writing—review and editing, D.B.S.; visualization, K.L.M.D.J. and C.E.F.M.; supervision, D.B.S.; project administration, D.B.S.; funding acquisition, D.B.S. All authors have read and agreed to the published version of the manuscript.

**Funding:** This research was funded by the Department of Science and Technology Philippine Council for Health Research and Development (DOST-PCHRD). The funded project titled D-HIVE 4B Capital.

**Institutional Review Board Statement:** Not applicable

**Informed Consent Statement:** Not applicable

**Data Availability Statement:** All data are contained in the manuscript.

**Acknowledgments:** This is to recognize the in-kind support of Mapua University, the Occidental Mindoro State College, and the Local Government Unit of San Jose, Occidental Mindoro.

**Conflicts of Interest:** The authors declare no conflict of interest.

## Abbreviations

Abbreviation/Symbol	Description
<i>AT</i>	Average Time
<i>BW</i>	Body Weight
<i>C<sub>d</sub></i>	Degree of Contamination
<i>CDI</i>	Chronic Daily Intake
<i>CI</i>	Contamination Index
<i>CV</i>	Coefficient of Variability
<i>EBK</i>	Empirical Bayesian Kriging
<i>ED</i>	Exposure Duration
<i>EF</i>	Exposure Frequency

<i>ELCR</i>	Excessive Lifetime Cancer Risk
<i>ERI</i>	Ecological Risk Index
<i>GIS</i>	Geographic Information System
<i>GPS</i>	Global Positioning System
<i>HEI</i>	Heavy Metal Evaluation Index
<i>HI</i>	Hazard Index
<i>HM</i>	Heavy Metal
<i>HN</i>	Hidden Neurons
<i>HQ</i>	Hazard Quotient
<i>HRA</i>	Health Risk Assessment
<i>IR</i>	Ingestion Rate
<i>LOD</i>	Limits of Detection
<i>MAS</i>	Metals Analysis System
<i>MLGI</i>	Machine Learning Geostatistical Interpolation
<i>MMs</i>	Metals and Metalloid
<i>MPI</i>	Metal Pollution Index
<i>N</i>	Number of Samples
<i>NCR</i>	Non-Carcinogenic Risk
<i>NI</i>	Number of Iterations
<i>NN-PSO</i>	Neural Network-Particle Swarm Optimization
<i>NP</i>	Number of Particles
<i>NPI</i>	Nemerow's Pollution Index
<i>PE</i>	Polyethylene
<i>PI</i>	Pollution Index
<i>PNSDW</i>	Philippine National Standards for Drinking Water
<i>RfD</i>	Reference Dose
<i>SD</i>	Standard Deviation
<i>SF</i>	Slope Factor
<i>T<sub>i</sub></i>	Toxic-Response Factor
<i>WRS</i>	Water Refilling Station
<i>WQ</i>	Water Quality
<i>XRF</i>	X-Ray Fluorescence

## Appendix A

**Table A1.** Metals and metalloids pollution and HRA studies in various regions of the world.

Continent	Country	Parameters Evaluated	Index Calculated	Results
	Bangladesh	Na, K, Ca, Mg, Mg, As, Fe, Mn, Cl, F, I, CO <sub>3</sub> , HCO <sub>3</sub> , NO <sub>3</sub> , PO <sub>4</sub>	WQI, HQ/HI, CR	8.69% (both pre- and post-monsoon) of the sampling sites have very poor WQI category; All sites have very high chronic risk during the pre-monsoon season, while that for post-monsoon is 20 of 23 sites; More than 70% of the sites have very high cancer risk during the pre-monsoon and the post-monsoon season [99].
Asia	Cambodia	Ag, Al, As, Ba, Cd, Co, Cr, Cu, Fe, Ga, Mn, Ni, Pb, Se, U, Zn	HQ/HI	HQ for As is the most significant element observed; Maximum value observed was HI = 3.57, which is greater than the threshold of 1.0 [100].

China	Cr <sup>6+</sup>	HQ/HI, CR	NCR shows induced risk for 7.47% and 12.07% of adults and children respectively, while that for CR shows 50.57% for adults and 16.67% for children [101].
India	Al, As, Cd, Co, Cr, Cu, Fe, Mn, Mo, Ni, Pb, V, Zn	HPI, HQ/HI, CR	Two sites have been identified as not suitable for drinking purposes without prior treatment; As is the most significant element to the NCR and CR in the area [102].
Iran	As, Cd, Cr	HI/HQ, CR	All sites have HQ > 1 considering As; Only one site has HQ < 1 considering Cr [103].
Iraq	As, Cr, Cu, Fe, Mn, Mo, Ni, Pb, Zn	HPI, HQ/HI, CR	28% of the sites exhibit HPI values within the category of Medium to Highly Polluted [104].
Jordan	Cd, Co, Cr, Li, Mn, Mo, Ni, Pb, U, V, Zn	CI, HQ/HI, CR	CR was within the acceptable risk limits [105].
Kazakhstan	Cd, Co, Cu, Fe, Mn, Ni, Pb, Zn	HPI, HQ/HI, CR	92.86% of the samples were considered to have a high level of pollution [106].
Korea	As, Cd, Cu, Pb, Zn	HQ/HI, CR	Water consumption on a frequent basis might potentially be detrimental due to long-term As exposure [107].
Kyrgyzstan	As, F	HQ/HI, CR	Children were observed to have a greater health risk than adults. Specifically, the CR of As via the oral intake pathway was above the permissible limits [108].
Lao PDR	As, B, Ba, Cr, Cu, Mn, Ni, Pb	HQ/HI, CR	Four sites observed HI > 1 and have CR above the acceptable risk level of $1 \times 10^{-4}$ [109].
Malaysia	SO <sub>4</sub> , Cl, Ca, Mg, Na, K, Al, Fe, Mn, Zn, Sr, As, Cr, Cd, Ni, Cu, Co, Pb	WQI	Some sampling sites were categorized as slightly polluted with HM concentrations exceeding the permissible limits [110].
Nepal	Ba, Cd, Co, Cr, Cu, Pb, Li, Mn, Mo, Ni, Sb, Sr, V, Zn	WQI, HQ/HI	WQI observed in the sampling sites was within the excellent water category; HQ values observed in the sampling sites were all less than 1, which suggested that it poses no adverse health effects to the residents [111].
Pakistan	F, Cl, Pb, Cd, Ni, Zn, Fe, As	HQ/HI, CR	HQ considering As has a value observed greater than 1, which suggests that it poses potential adverse health effects in the residents; 3.3% of the sites have CR values above the USEPA threshold limit [112].
Philippines	As, Ba, Cu, Fe, Pb, Mn, Ni, Zn	HPI, NPI, HQ/HI, CR	All sampling locations were categorized to have a high level of pollution; CR via ingestion pathway exceeded the USEPA threshold limit [30].
Saudi Arabia	Ag, Al, B, Ba, Cr, Cu, Fe,	HPI, Cd, HQ/HI	Potential NCR showed that HQ for Al, Mo, Cu, Cr, and Pb exceeded the

	Mo, Ni, Pb, V, Zn		recommended value of 1, implying that it can cause a potential adverse health effect [113].
Thailand	Ca <sup>2+</sup> , Mg <sup>2+</sup> , Na, K, Fe, SO <sub>4</sub> <sup>2-</sup> , NO <sub>3</sub> <sup>-</sup> , Cl <sup>-</sup> , HCO <sub>3</sub> <sup>-</sup>	HQ/HI, CR	Study showed that As is the most significant element with respect to the NCR and chronic effects, and was predominant with adults [114].
United Arab Emirates	Cl <sup>-</sup> , SO <sub>4</sub> <sup>2-</sup> , Ca <sup>2+</sup> , Na <sup>+</sup> , K <sup>+</sup> , Mg <sup>2+</sup> , Ba <sup>2+</sup> , As, Cd, Pb, Cr, Cu, Zn	HQ/HI	30% of the sites were classified to have a very high risk [115].
Vietnam	As	CR	Skin CR is 11.5 times greater in unfiltered water and 14.8 times higher when consuming water for a lifetime that has been exposed to As [116].
Algeria	Cd, Cr, Cu, Mn, Ni, Pb, Zn	HPI, HEI	HPI values observed for all samples were below the critical value; No chronic HR was posed by the GW [117].
Cameroon	As, Cd, Co, Cr, Cu, Ni, Pb, Zn	WQI, HPI, HEI, HQ/HI, CR	WQI suggests that the GW is categorized to be poor to unsuitable; HM concentrations presented a risk for non-carcinogenic health consequences; Ingestion of groundwater also posed a moderate to high risk of developing cancer in both adults and children [118].
Egypt	Fe, Mn, Pb, Cd, Ni, Cu, Zn, Cr, As	HQ/HI, CR	Ingestion is observed to be the most significant pathway of exposure; The prevalence of arsenic was stated to be accountable for the highest CR [119].
Ethiopia	Pb	HQ/HI, CR	Mean HQ levels both for children and adults were below 1; CR values for adults and children were within the permissible levels of USEPA [120].
Africa	Na <sup>+</sup> , K <sup>+</sup> , Ca <sup>2+</sup> , Mg <sup>2+</sup> , HCO <sub>3</sub> <sup>-</sup> , F <sup>-</sup> , Cl <sup>-</sup> , NO <sub>3</sub> <sup>-</sup> , PO <sub>4</sub> <sup>3-</sup> , SO <sub>4</sub> <sup>2-</sup> , Pb <sup>2+</sup> , Co, Cr, Fe, Mn, Zn, Cu, Cd	HQ/HI, CR	HQ due to Mn and Fe was greater than 1, implying that it can cause a potential adverse health effect [121].
Kenya	Cd, Ni, Pb	HPI, HEI, HQ/HI, CR	All samples had hazard indices that exceeded 1, which indicated a significant risk due to the metal exposure; CR values were greater than the USEPA permissible limit for both children and adults [122].
Morocco	Cd, Cr, Cu, Fe, Mn, Ni, Pb, Zn	HQ/HI	HQ was significantly influenced by Zn concentration [123].
Mozambique	Sr, Li, B, Al, Ba, V, Mn, Fe, Hg, Co, Ni, Cu, Pb, Zn, As, Rb, U	HQ/HI	HQ values exceed the maximum permissible limit for children due to ingestion pathway [124].

	Nigeria	Cl, Fe, Zn, Pb, Cu, Ni, Cr, Mn, Cd	WQI, ERI, HEI, HPI, HQ/HI, CR	About 24% of the samples have deteriorated water quality; About 15% of the samples posed moderate ecological risks; Cu is the most significant element to the HI and more than 40% of the samples presented high chronic HR; High Cr risk was observed in 19% of the samples, while that for Cd and Ni is 14% [3].
	Senegal	Pb, Cd, Cu, Fe, Mn	HQ/HI	High risk for infants and children with respect to Pb and Cd [125].
	South Africa	Ag, Al, B, Cd, Co, Cu, Fe, Li, Mn, Li, Mn, Ni, Pb, Si, Zn	HPI, HQ/HI	Two zones presented high contamination classification based on their HPI values; All age groups were exposed to potential health risks due to HQ via ingestion pathway [126].
	Sudan	CO <sub>3</sub> <sup>2-</sup> , HCO <sub>3</sub> <sup>-</sup> , NO <sub>3</sub> <sup>-</sup> , NO <sub>2</sub> <sup>-</sup> , SO <sub>4</sub> <sup>2-</sup> , NH <sub>3</sub> , F, Cl <sup>-</sup> , Na <sup>+</sup> , K <sup>+</sup> , Mg <sup>2+</sup> , Ca <sup>2+</sup>	HQ/HI	About 60% of the sampling sites presented potential health risks for both children and adults [127].
	Argentina	Ca <sup>2+</sup> , Mg <sup>+</sup> , K <sup>+</sup> , HCO <sub>3</sub> <sup>-</sup> , Cl <sup>-</sup> , SO <sub>4</sub> <sup>2-</sup> , NO <sub>3</sub> <sup>-</sup> , Cr(IV)	HQ/HI, CR	HQ value via ingestion pathway is greater than 1 for both adults and children; CR due to Cr(VI) exceeded the permissible limit set by the USEPA [128].
	Brazil	Ca, Mg, Na, K, Cl <sup>-</sup> , HCO <sub>3</sub> <sup>-</sup> , SO <sub>4</sub> <sup>2-</sup> , NH <sub>4</sub> <sup>+</sup> , NO <sub>3</sub> <sup>-</sup> , F <sup>-</sup> , Fe, Mn	WQI, HPI	WQI and HPI values presented samples that were of good quality [129].
	Ecuador	Al, Ba, Ca, Fe, K, Mg, Mn, Na, Sr, Cu, Cr, Pb, Zn	HPI	6.6% of the samples in a sampling region have Pb levels above the threshold value [130].
North and South America	Mexico	As, F	HQ/HI	Observed HI > 1 for both adults and children suggests a potential health risk and was attributed to exposure to As and F [131].
	Paraguay/Uruguay/Argentina/Bolivia	Li, B, Al, Si, V, Cr(III), Mn, Fe, Co, Ni, Cu, As, Rb, Sr, Cd, Cs, Ba, Pb, U	HPI, HQ/HI	34 sites were categorized as highly polluted sites; HQ value calculated indicated no risk [132].
	Peru	Au, Cd, Co, Cr, Cu, Fe, Mn, Mo, Ni, Pd, Pt, Sc, Ti, V, Zn, Al, Pb, Sn, As, B, Ge, Si, Er, Nd, Yb, P, Se, Ba, Ca, K, Li, Mg, Sr	HQ/HI, CR	As is the most significant CR. HQ via ingestion for As, B, Zn, Cu, Ba, and Sr were major contributors to the NCR [133].
Europe	Czech Republic	Cr <sup>total</sup> , Zn, Pb, Cd, Hg	HEI, HPI	All samples were below the threshold value [134].

	Greece	Cr(VI), NO <sub>3</sub> -N	HQ/HI	HQ was acceptable for all sites considering adults; one site has HQ > 1 for children, suggesting potential adverse health effects; multiple sites have CR greater than the permissible limit by the USEPA [135].
	Italy	Al, As, Ba, Cd, Cr, Cu, Fe, Mn, Ni, Pb, Se, Zn	HPI	HPI values were within the critical pollution level category [136].
	Poland	Pb, Cd, Ni, Cu, Fe, Zn, NH <sub>4</sub>	NPI, HQ/HI	High risk of contamination due to Pb and Cu [137].
	Romania	NH <sub>4</sub> <sup>+</sup> , HCO <sub>3</sub> <sup>-</sup> , Cl <sup>-</sup> , NO <sub>3</sub> <sup>-</sup> , NO <sub>2</sub> <sup>-</sup> , SO <sub>4</sub> <sup>2-</sup> , Li, Na, Mg, Al, K, Ca, Sr, Ba, Mn, Fe, Cu, Zn, Ga	WQI, HEI, HPI, Ca, HQ/HI	WQI values suggested water classification as marginal, poor, and very poor quality; Cl <sup>-</sup> , Al, and NO <sub>3</sub> <sup>-</sup> were the most significant parameters in the exceedance of HQ to the permissible limit; Fe and Li were the dominant contributors to HPI value [138].
	Serbia	Al, As, Cu, Zn, Fe, Cr, Cd, Mn, Ni, Pb, Hg	HQ/HI	HQ due to As and Hg in multiple sites suggested potential non-carcinogenic health effects [139].
	Ukraine	Al, As, Cr, Cd, Cu, Mn, Ni, Pb, Zn	HPI, HEI, HQ/HI	17% of the samples have HI > 1, suggesting potential non-carcinogenic health effects [140]
Oceania	Fiji	Cd, Cr, Mn, Ni, Pb, Zn	HQ/HI	HI > 1 for all sites both for children and adults, posing potential health risk; CR of Cd is higher compared to other metals in all sites, exceeding the USEPA threshold limit [141].
	Papua New Guinea	Ca, Mg, Mn	WQI	14% of the samples have poor quality [142].

## Appendix B

**Table A2.** Coordinates of the Sampling Points for DW.

Sampling Point Code	Barangay	Latitude (° N)	Longitude (° E)	Elevation
SJ-B01-DW1	Bagong Sikat	12.367	121.069	4.0 m
SJ-B04-DW2	Barangay II Pob.	12.353	121.066	7.0 m
SJ-B05-DW3	Barangay III Pob.	12.355	121.061	7.0 m
SJ-B05-DW3	Barangay III Pob.	12.358	121.068	1.0 m
SJ-B05-DW3	Barangay III Pob.	12.356	121.066	8.0 m
SJ-B06-DW4	Barangay IV Pob.	12.351	121.061	5.0 m
SJ-B08-DW5	Barangay VI Pob.	12.353	121.066	7.0 m
SJ-B11-DW6	Batasan	12.527	121.119	85.0 m
SJ-B12-DW7	Bayotbot	12.405	121.098	19.0 m
SJ-B13-DW8	Bubog	12.366	121.038	8.0 m
SJ-B13-DW8	Bubog	12.371	121.033	9.0 m
SJ-B14-DW9	Buri	12.223	121.094	163.0 m
SJ-C01-DW10	Camburay	12.427	121.097	26.0 m
SJ-C01-DW10	Camburay	12.429	121.097	28.0 m

SJ-C01-DW10	Camburay	12.430	121.095	28.0 m
SJ-C04-DW11	Central	12.434	121.048	20.0 m
SJ-C04-DW11	Central	12.457	121.041	27.0 m
SJ-C04-DW11	Central	12.449	121.032	18.0 m
SJ-I01-DW12	Iling Proper	12.245	121.088	144.0 m
SJ-I03-DW13	Ipil	12.253	121.091	17.0 m
SJ-L01-DW14	La Curva	12.410	121.016	6.0 m
SJ-L01-DW14	La Curva	12.403	121.071	13.0 m
SJ-L02-DW15	Labangan Iling	12.292	121.050	15.0 m
SJ-L03-DW16	Labangan Poblacion	12.355	121.069	8.0 m
SJ-L03-DW16	Labangan Poblacion	12.365	121.075	5.0 m
SJ-M01-DW17	Mabini	12.372	121.086	7.0 m
SJ-M01-DW17	Mabini	12.368	121.098	8.0 m
SJ-M02-DW18	Magbay	12.409	121.089	20.0 m
SJ-M03-DW19	Mangarin	12.360	121.102	7.0 m
SJ-M03-DW19	Mangarin	12.352	121.100	0.0 m
SJ-M03-DW19	Mangarin	12.352	121.099	7.0 m
SJ-M06-DW21	Murtha	12.471	121.117	47.0 m
SJ-M06-DW21	Murtha	12.436	121.108	25.0 m
SJ-M06-DW21	Murtha	12.440	121.103	28.0 m
SJ-M06-DW22	Murtha	12.457	121.118	36.0 m
SJ-N02-DW23	Natandol	12.184	121.106	55.0 m
SJ-P02-DW24	Pawican	12.171	121.119	99.0 m
SJ-S01-DW25	San Agustin	12.444	121.022	16.0 m
SJ-S02-DW26	San Isidro	12.417	121.057	13.0 m
SJ-S03-DW27	San Roque	12.358	121.051	4.0 m
SJ-A02-DW01	Ansiray	12.273	121.078	13.0 m
SJ-B01-DW02	Bagong Sikat	12.367	121.069	4.0 m
SJ-B02-DW03	Bangkal	12.224	121.049	5.0 m
SJ-B04-DW04	Barangay II	12.353	121.066	7.0 m
SJ-B05-DW05	Barangay III	12.356	121.066	8.0 m
SJ-B06-DW06	Barangay IV Pob.	12.351	121.061	5.0 m
SJ-B06-DW07	Barangay VI Pob.	12.353	121.066	7.0 m
SJ-B11-DW08	Batasan	12.527	121.118	71.0 m
SJ-B12-DW09	Bayotbot	12.405	121.098	19.0 m
SJ-B13-DW10	Bubog	12.366	121.039	9.0 m
SJ-C01-DW11	Camburay	12.429	121.097	28.0 m
SJ-C04-DW12	Central	12.433	121.048	16.0 m
SJ-C04-DW13	Central	12.457	121.041	27.0 m
SJ-I01-DW14	Iling Proper	12.253	121.034	20.0 m
SJ-I01-DW15	Iling Proper	12.248	121.036	26.0 m
SJ-I02-DW16	Inasakan	12.216	121.069	16.0 m
SJ-L01-DW17	La Curva	12.410	121.082	18.0 m
SJ-L01-DW18	La Curva	12.403	121.071	13.0 m
SJ-L02-DW19	Labangan Iling	12.290	121.049	52.0 m
SJ-L03-DW20	Labangan Poblacion	12.365	121.075	5.0 m
SJ-M01-DW21	Mabini	12.372	121.086	7.0 m
SJ-M01-DW22	Mabini	12.368	121.100	8.0 m
SJ-M02-DW23	Magbay	12.409	121.089	20.0 m
SJ-M03-DW24	Mangarin	12.360	121.102	7.0 m
SJ-M03-DW25	Mangarin	12.352	121.099	7.0 m

SJ-M05-DW26	Monteclaro	12.547	121.125	75.0 m
SJ-M06-DW27	Murtha	12.471	121.117	47.0 m
SJ-M06-DW28	Murtha	12.440	121.103	28.0 m
SJ-S01-DW29	San Agustin	12.444	121.023	16.0 m
SJ-S02-DW30	San Isidro	12.417	121.057	13.0 m
SJ-S03-DW31	San Roque	12.358	121.051	4.0 m

**Table A3.** Coordinates of the Sampling Points for GW.

Sampling Point Code	Barangay	Latitude (° N)	Longitude (° E)	Elevation
SJ-B11-GW1	Batasan	12.527	121.119	85.0 m
SJ-B12-GW2	Bayotbot	12.405	121.098	19.0 m
SJ-B13-GW3	Bubog	12.365	121.038	8.0 m
SJ-B13-GW4	Bubog	12.266	121.038	48.0 m
SJ-B13-GW5	Bubog	12.371	121.033	9.0 m
SJ-B14-GW6	Buri	12.223	121.094	163.0 m
SJ-C01-GW7	Camburay	12.492	121.095	144.0 m
SJ-C04-GW8	Central	12.434	121.048	20.0 m
SJ-C04-GW9	Central	12.457	121.041	27.0 m
SJ-C04-GW10	Central	12.449	121.032	18.0 m
SJ-I01-GW11	Iling Proper	12.245	121.088	144.0 m
SJ-I03-GW12	Ipil	12.253	121.091	17.0 m
SJ-L01-GW13	La Curva	12.410	121.082	18.0 m
SJ-L01-GW14	La Curva	12.412	121.085	20.0 m
SJ-L01-GW15	La Curva	12.403	121.071	13.0 m
SJ-L02-GW16	Labangan Iling	12.292	121.050	15.0 m
SJ-L03-GW17	Labangan Poblacion	12.361	121.078	7.0 m
SJ-M01-GW18	Mabini	12.372	121.086	7.0 m
SJ-M01-GW19	Mabini	12.368	121.100	8.0 m
SJ-M02-GW20	Magbay	12.409	121.089	20.0 m
SJ-M03-GW21	Mangarin	12.360	121.102	7.0 m
SJ-M03-GW22	Mangarin	12.352	121.100	0.0 m
SJ-M03-GW23	Mangarin	12.352	121.099	7.0 m
SJ-M06-GW25	Murtha	12.471	121.117	47.0 m
SJ-M06-GW26	Murtha	12.436	121.108	25.0 m
SJ-M06-GW27	Murtha	12.440	121.103	28.0 m
SJ-M06-GW28	Murtha	12.445	121.105	31.0 m
SJ-N02-GW29	Natandol	12.184	121.106	55.0 m
SJ-P02-GW30	Pawican	12.171	121.119	99.0 m
SJ-S01-GW31	San Agustin	12.444	121.022	16.0 m
SJ-S02-GW32	San Isidro	12.417	121.057	13.0 m

## Appendix C

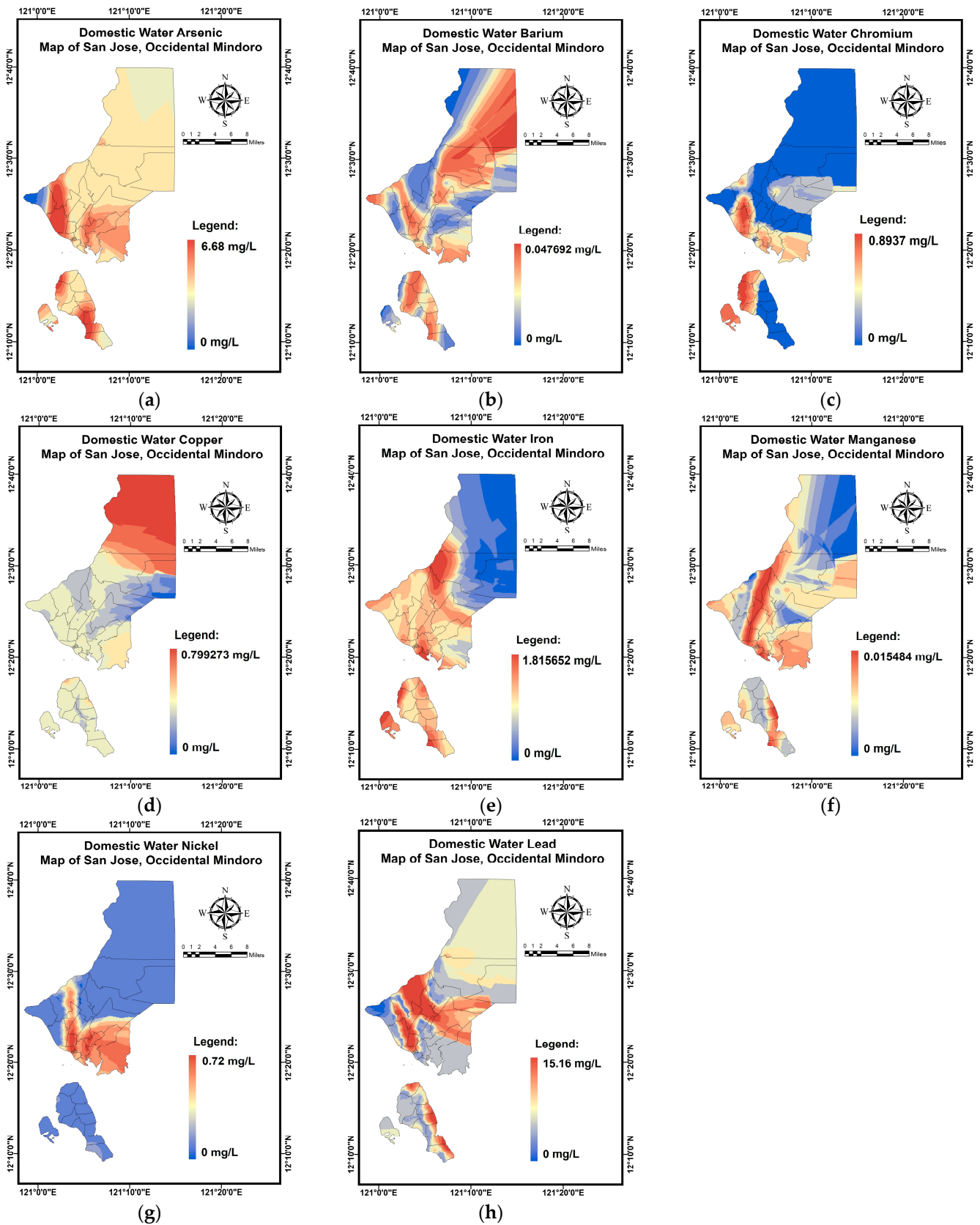


Figure A1. MLGI spatial maps of the (a) As; (b) Ba; (c) Cr; (d) Cu; (e) Fe; (f) Mn; (g) Ni; (h) Pb in domestic water.

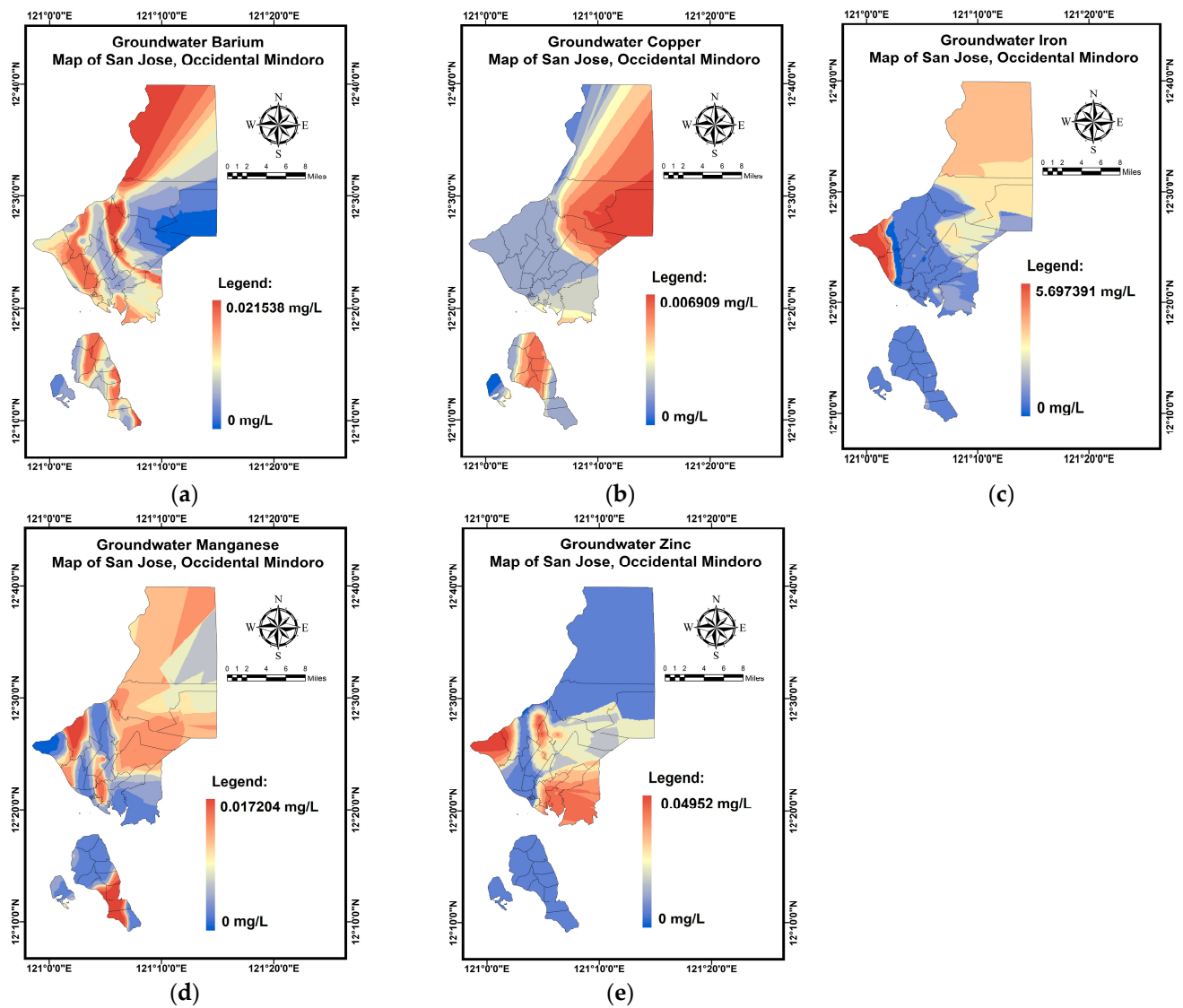


Figure A2. MLGI spatial maps of the (a) Ba; (b) Cu; (c) Fe; (d) Mn; (e) Zn in GW.

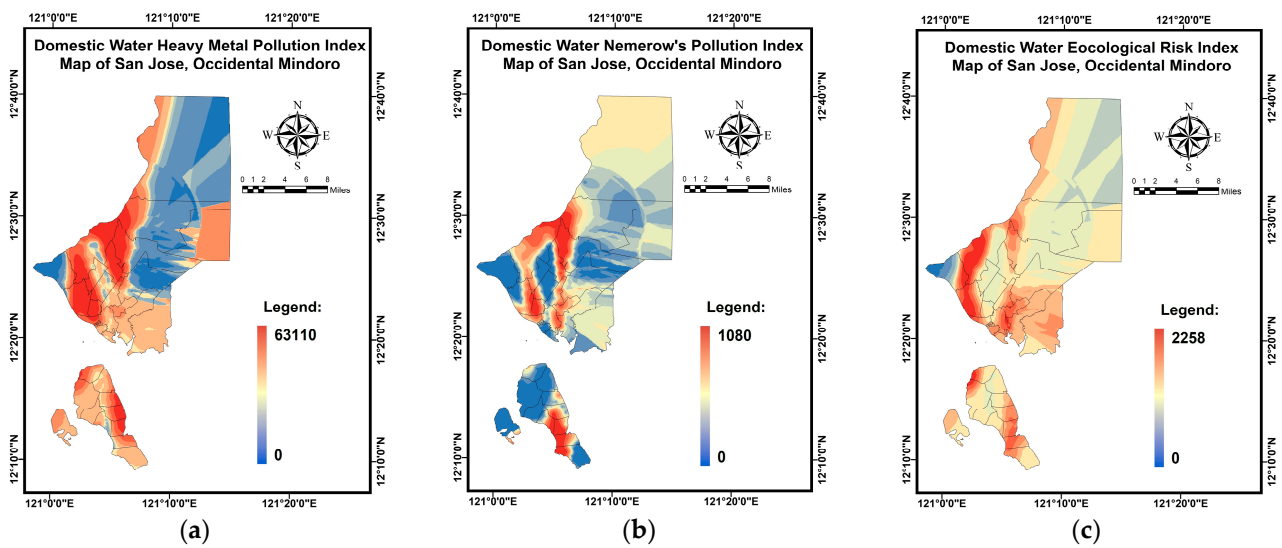


Figure A3. MLGI spatial maps of the (a) HPI; (b) NPI; (c) ERI in DW.

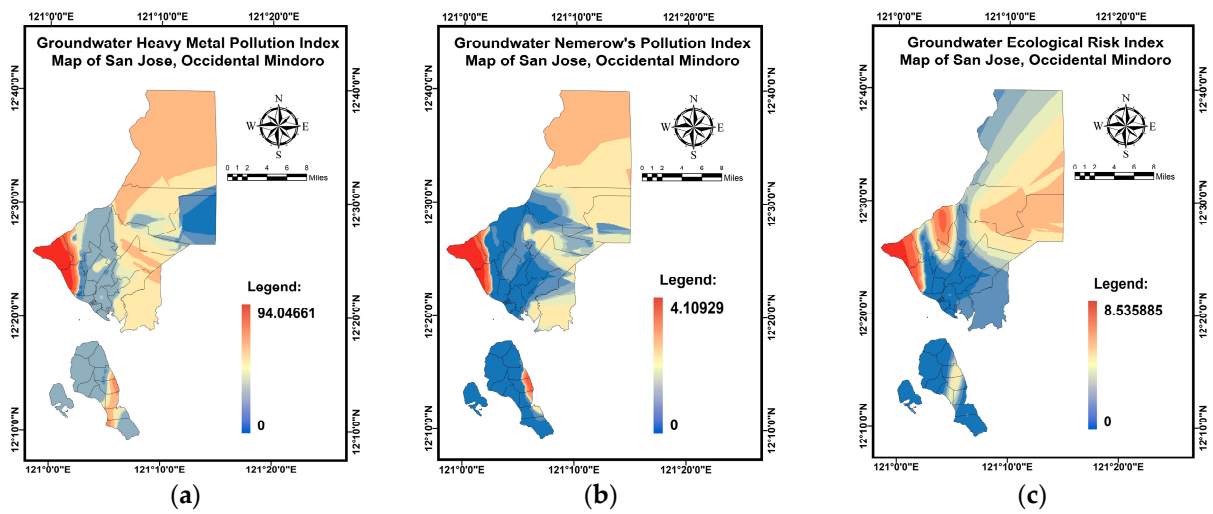
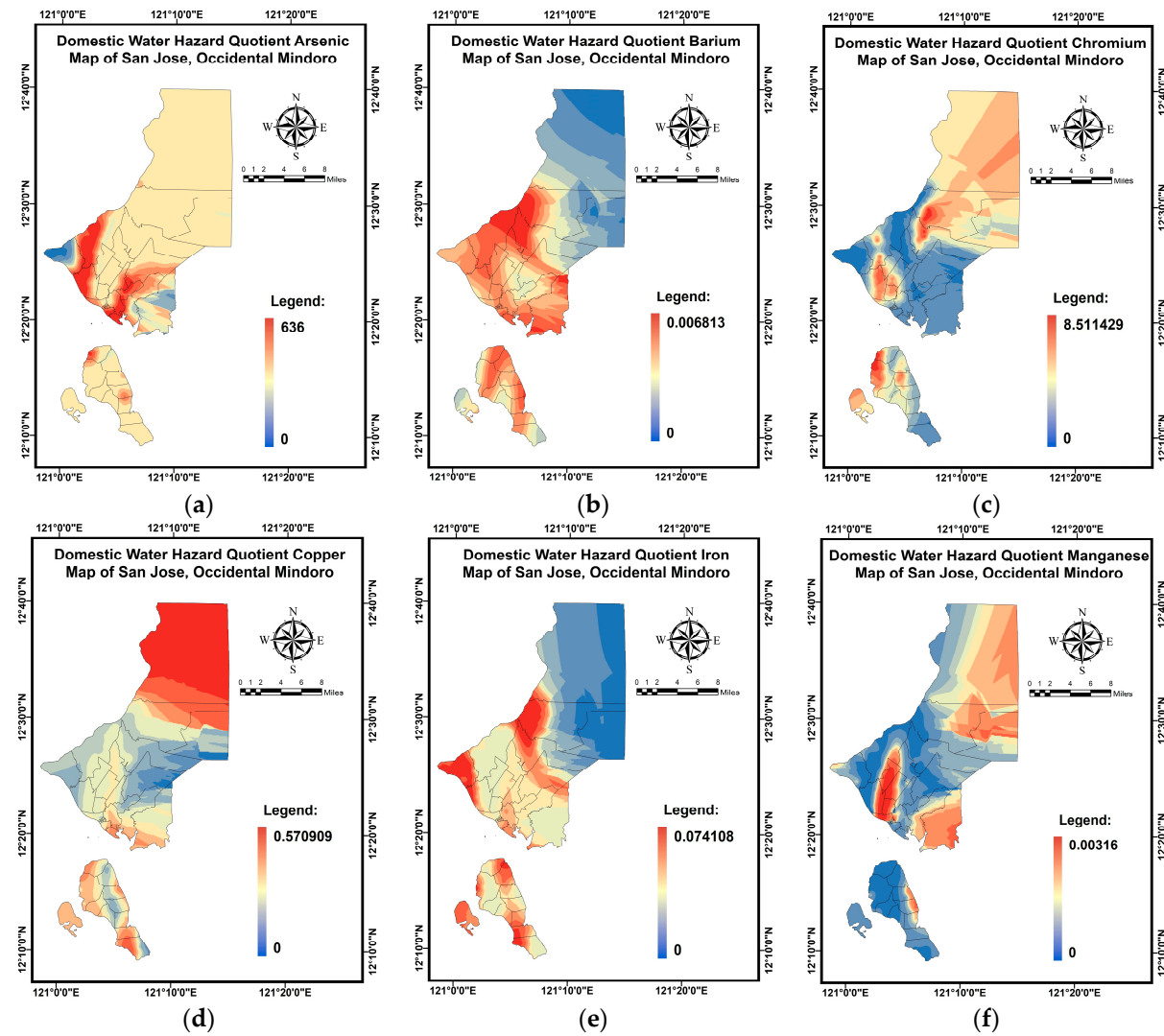


Figure A4. MLGI spatial maps of the (a) HPI; (b) NPI; (c) ERI in groundwater.



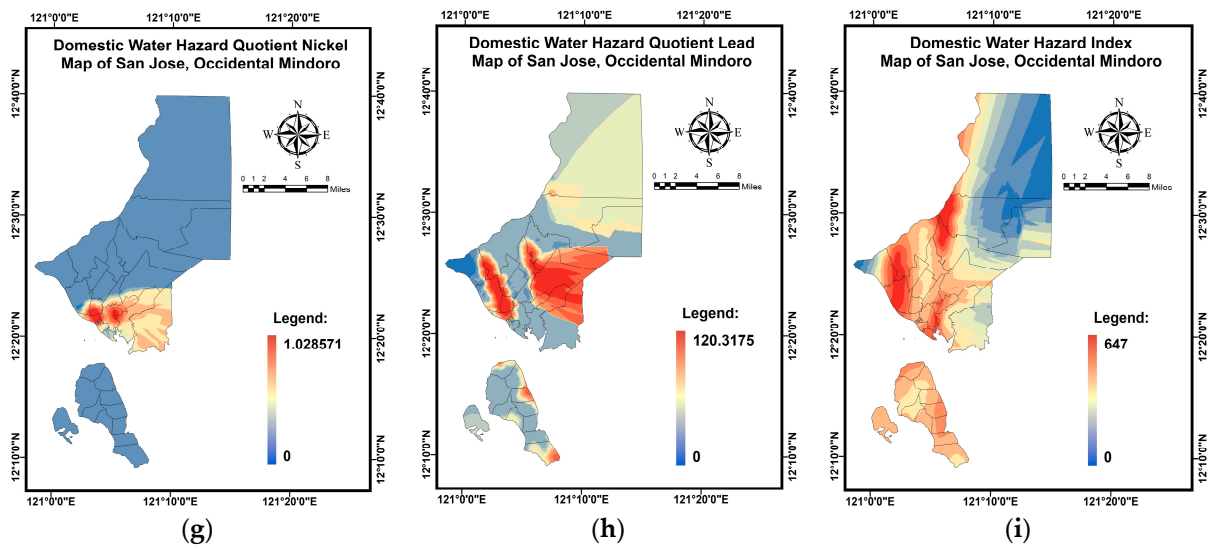


Figure A5. MLGI spatial maps of the (a) HQ (As); (b) HQ (Ba); (c) HQ (Cr); (d) HQ (Cu); (e) HQ (Fe); (f) HQ (Mn); (g) HQ (Ni); (h) HQ (Pb); (i) HI in domestic water.

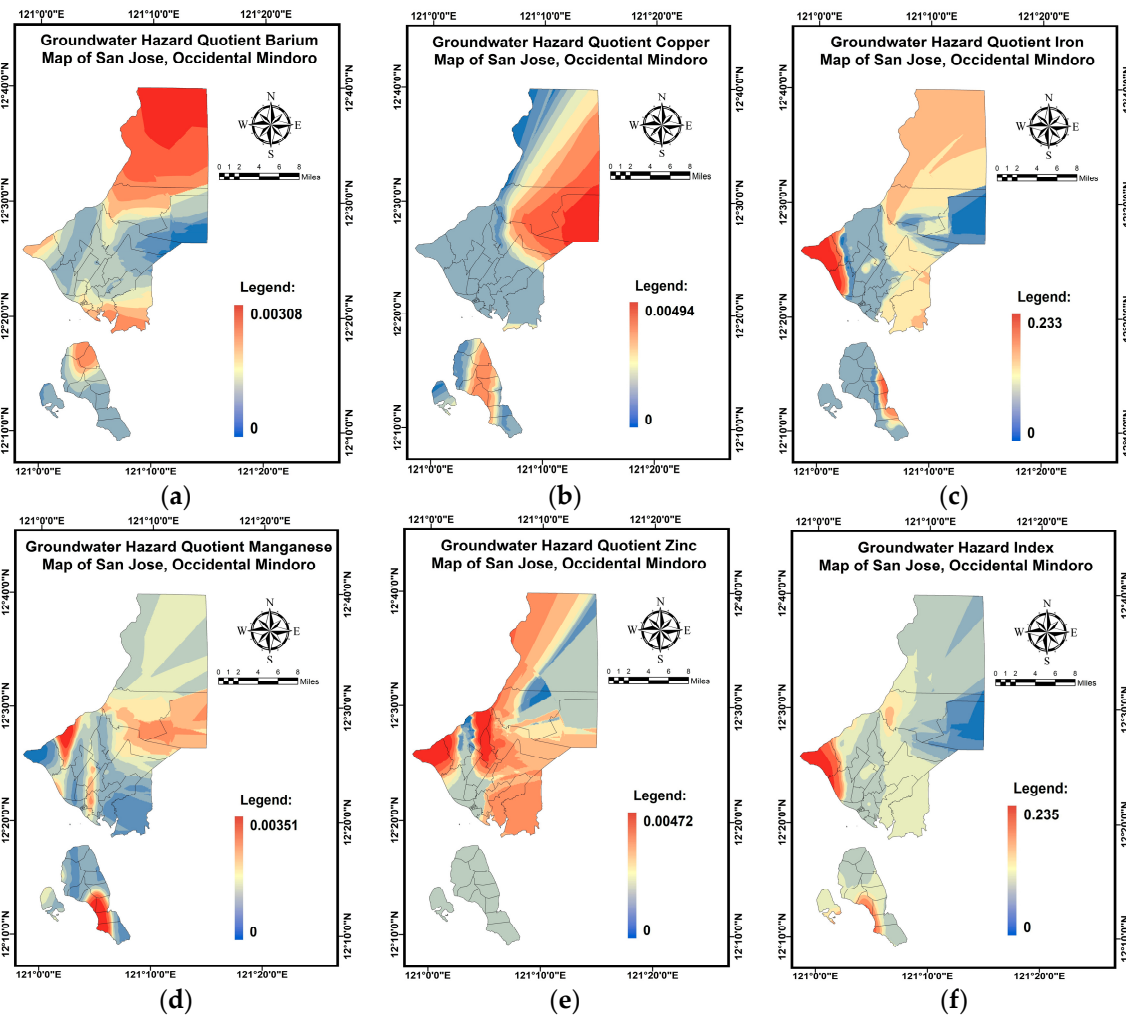
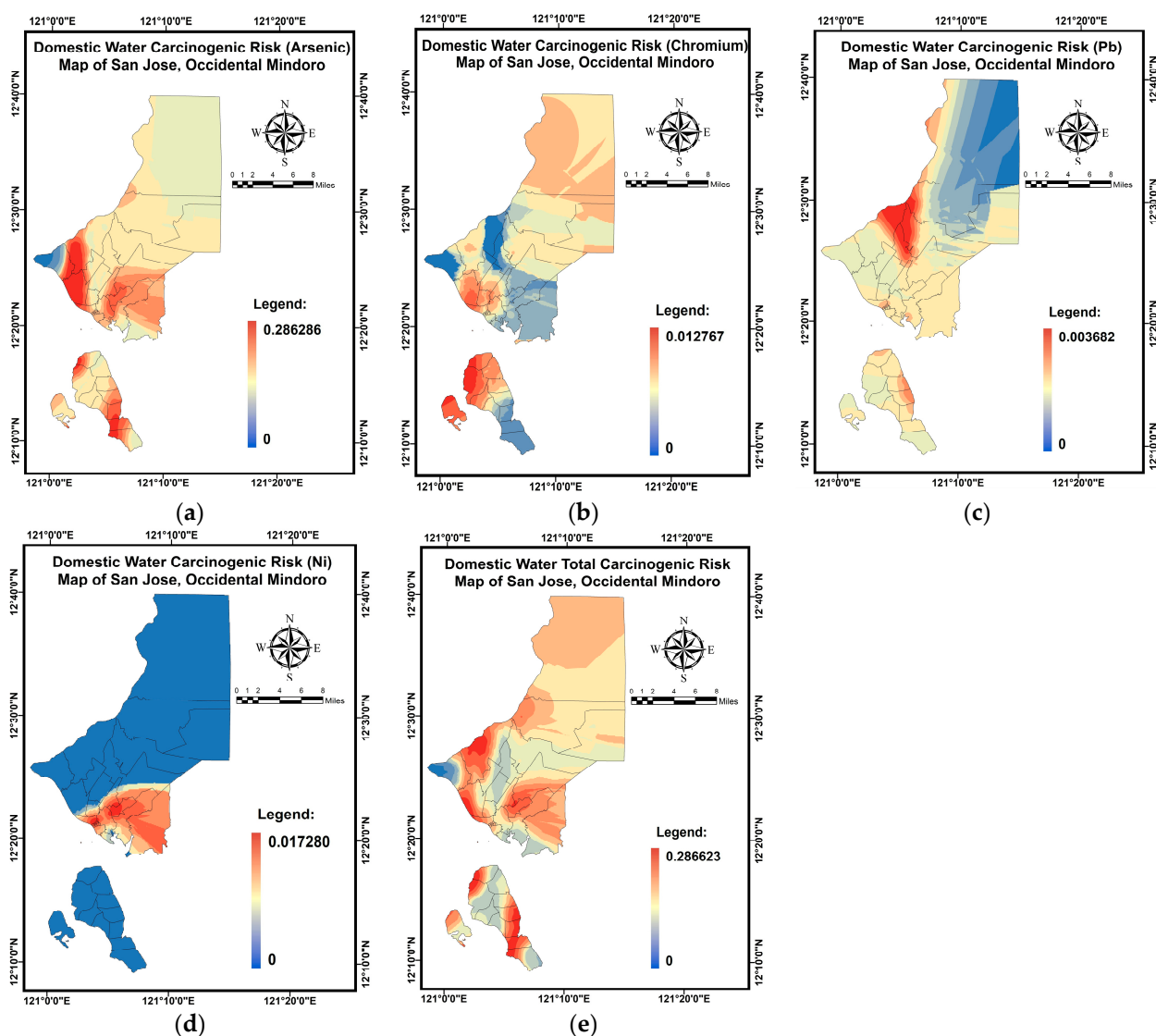


Figure A6. MLGI spatial maps of the (a) HQ (Ba); (b) HQ (Cu); (c) HQ (Fe); (d) HQ (Mn); (e) HQ (Zn); (f) HI in groundwater.



**Figure A7.** MLGI spatial maps of the (a) Cr (As); (b) CR (Cr); (c) CR (Pb); (d) CR (Ni); (e) TCR in domestic water.

## References

- Bhattacharya, S.; Das, S.; Das, S.; Kalashetty, M.; Warghat, S.R. An integrated approach for mapping groundwater potential applying geospatial and MIF techniques in the semiarid region. *Environ. Dev. Sustain.* **2021**, *23*, 495–510.
- Kumar, V.; Parihar, R.D.; Sharma, A.; Bakshi, P.; Singh Sidhu, G.P.; Bali, A.S.; Karaouzas, I.; Bhardwaj, R.; Thukral, A.K.; Gyasi-Agyei, Y.; et al. Global Evaluation of Heavy Metal Content in Surface Water Bodies: A Meta-Analysis Using Heavy Metal Pollution Indices and Multivariate Statistical Analyses. *Chemosphere* **2019**, *236*, 124364.
- Ukah, B.U.; Egbueri, J.C.; Unigwe, C.O.; Ubido, O.E. Extent of heavy metals pollution and health risk assessment of groundwater in a densely populated industrial area, Lagos, Nigeria. *Int. J. Energy Water Resour.* **2019**, *3*, 291–303.
- Mirzabeygi, M.; Abbasnia, A.; Yunesian, M.; Nodehi, R.N.; Yousefi, N.; Hadi, M.; Mahvi, A.H. Heavy metal contamination and health risk assessment in drinking water of Sistan and Baluchistan, Southeastern Iran. *Hum. Ecol. Risk Assess. Int. J.* **2017**, *23*, 1893–1905.
- Mohammadi, A.A.; Zarei, A.; Majidi, S.; Ghaderpoury, A.; Hashempour, Y.; Saghi, M.H.; Alinejad, A.; Yousefi, M.; Hosseingholizadeh, N.; Ghaderpoori, M. Carcinogenic and non-carcinogenic health risk assessment of heavy metals in drinking water of Khorramabad, Iran. *MethodsX* **2019**, *6*, 1642–1651.
- Hoang, H.G.; Lin, C.; Tran, H.T.; Chiang, C.F.; Bui, X.T.; Cheruiyot, N.K.; Shern, C.C.; Lee, C.W. Heavy metal contamination trends in surface water and sediments of a river in a highly-industrialized region. *Environ. Technol. Innov.* **2020**, *20*, 101043.
- Yeh, G.; Lin, C.; Nguyen, D.H.; Hoang, H.G.; Shern, J.C.; Hsiao, P.J. A five-year investigation of water quality and heavy metal mass flux of an industrially affected river. *Environ. Sci. Pollut. Res.* **2021**, *29*, 12465–12472.

8. Yousefi, M.; Ghalehaskar, S.; Asghari, F.B.; Ghaderpoury, A.; Dehghani, M.H.; Ghaderpoori, M.; Mohammadi, A.A. Distribution of fluoride contamination in drinking water resources and health risk assessment using geographic information system, north-west Iran. *Regul. Toxicol. Pharmacol.* **2019**, *107*, 104408.
9. Zhang, Y.; Xu, B.; Guo, Z.; Han, J.; Li, H.; Jin, L.; Chen, F.; Xiong, Y. Human health risk assessment of groundwater arsenic contamination in Jinghui irrigation district, China. *J. Environ. Manag.* **2019**, *237*, 163–169.
10. Peana, M.; Medici, S.; Dadar, M.; Zoroddu, M.A.; Pelucelli, A.; Chasapis, C.T.; Bjørklund, G. Environmental barium: Potential exposure and health-hazards. *Arch. Toxicol.* **2021**, *95*, 2605–2612.
11. Miah, M.R.; Ijomone, O.M.; Okoh, C.O.; Ijomone, O.K.; Akingbade, G.T.; Ke, T.; Krum, B.; da Cunha Martins Jr, A.; Akinyemi, A.; Aranoff, N.; et al. The effects of manganese overexposure on brain health. *Neurochem. Int.* **2020**, *135*, 104688.
12. Grzeszczak, K.; Kwiatkowski, S.; Kosik-Bogacka, D. The role of Fe, Zn, and Cu in pregnancy. *Biomolecules* **2020**, *10*, 1176.
13. Long, X.; Liu, F.; Zhou, X.; Pi, J.; Yin, W.; Li, F.; Huang, S.; Ma, F. Estimation of spatial distribution and health risk by arsenic and heavy metals in shallow groundwater around Dongting Lake plain using GIS mapping. *Chemosphere* **2021**, *269*, 128698.
14. Mahapatra, S.R.; Venugopal, T.; Shanmugasundaram, A.; Giridharan, L.; Jayaprakash, M. Heavy metal index and geographical information system (GIS) approach to study heavy metal contamination: A case study of north Chennai groundwater. *Appl. Water Sci.* **2020**, *10*, 1–17.
15. Saleh, H.N.; Panahande, M.; Yousefi, M.; Asghari, F.B.; Oliveri Conti, G.; Talaei, E.; Mohammadi, A.A. Carcinogenic and non-carcinogenic risk assessment of heavy metals in groundwater wells in Neyshabur Plain, Iran. *Biol. Trace Elem. Res.* **2019**, *190*, 251–261.
16. Gad, M.; El-Safa, A.; Magda, M.; Farouk, M.; Hussein, H.; Alnemari, A.M.; Elsayed, S.; Khalifa, M.M.; Moghanm, F.S.; Eid, E.M.; et al. Integration of water quality indices and multivariate modeling for assessing surface water quality in Qaroun Lake, Egypt. *Water* **2021**, *13*, 2258.
17. Cüce, H.; Kalıpcı, E.; Ustaoglu, F.; Kaynar, I.; Baser, V.; Türkmen, M. Multivariate statistical methods and GIS based evaluation of the health risk potential and water quality due to arsenic pollution in the Kızılırmak River. *Int. J. Sediment Res.* **2022**, *37*, 754–765.
18. Yüksel, B.; Ustaoglu, F.; Arica, E. Impacts of a garbage disposal facility on the water quality of çavuşlu stream in Giresun, Turkey: A health risk assessment study by a validated ICP-MS assay. *Aquat. Sci. Eng.* **2021**, *36*, 181–192.
19. Bushero, D.M.; Angello, Z.A.; Behailu, B.M. Evaluation of hydrochemistry and identification of pollution hotspots of little Akaki river using integrated water quality index and GIS. *Environ. Chall.* **2022**, *8*, 100587.
20. Nath, B.K.; Chaliha, C.; Bhuyan, B.; Kalita, E.; Baruah, D.C.; Bhagabati, A.K. GIS mapping-based impact assessment of groundwater contamination by arsenic and other heavy metal contaminants in the Brahmaputra River valley: A water quality assessment study. *J. Clean. Prod.* **2018**, *201*, 1001–1011.
21. San Jose, Province of Occidental Mindoro. Available online: <https://www.philatlas.com/luzon/mimaropa/occidental-mindoro/san-jose.html> (accessed on 14 January 2023).
22. Municipality of San Jose, Province of Occidental Mindoro. Available online : <https://www.occidentalmindoro.gov.ph/san-jose/> (accessed on 14 January 2023).
23. Executive Summary of San Jose, Province of Occidental Mindoro. Available online: <https://coa.gov.ph/download/5184/occidental-mindoro/71786/san-jose-executive-summary-2021-6.pdf> (accessed on 14 January 2023).
24. Climate Change-Responsive Integrated River Basin Management and Development Master Plans for the 8 Clustered River Basins. Available online: <https://riverbasin.denr.gov.ph/masterplans/8Cluster%20Executive%20Summary/RBCOCluster3ExecutiveSummary.pdf> (accessed on 14 January 2023).
25. Municipal Planning and Development Office. *Municipality of San Jose, Province of Occidental Mindoro—Comprehensive Land and Water Use Plan 2017-2030*; Municipal Planning and Development Office: San Jose, Philippines, 2017; Volume 1.
26. de Jesus, K.L.M.; Senoro, D.B.; Dela Cruz, J.C.; Chan, E.B. A Hybrid Neural Network–Particle Swarm Optimization Informed Spatial Interpolation Technique for Groundwater Quality Mapping in a Small Island Province of the Philippines. *Toxics* **2021**, *9*, 273.
27. Melquiades, F.L.; Appoloni, C. Application of XRF and field portable XRF for environmental analysis. *J. Radioanal. Nucl. Chem.* **2004**, *262*, 533–541.
28. Zhou, S.; Yuan, Z.; Cheng, Q.; Zhang, Z.; Yang, J. Rapid in situ determination of heavy metal concentrations in polluted water via portable XRF: Using Cu and Pb as example. *Environ. Pollut.* **2018**, *243*, 1325–1333.
29. Wu, C.M.; Tsai, H.T.; Yang, K.H.; Wen, J.C. How reliable is X-ray fluorescence (XRF) measurement for different metals in soil contamination? *Environ. Forensics* **2012**, *13*, 110–121.
30. Senoro, D.B.; de Jesus, K.L.M.; Nolos, R.C.; Lamac, M.R.L.; Deseo, K.M.; Tabelin, C.B. In Situ Measurements of Domestic Water Quality and Health Risks by Elevated Concentration of Heavy Metals and Metalloids Using Monte Carlo and MLGI Methods. *Toxics* **2022**, *10*, 342.
31. Senoro, D.B.; de Jesus, K.L.M.; Mendoza, L.C.; Apostol, E.M.D.; Escalona, K.S.; Chan, E.B. Groundwater quality monitoring using in-situ measurements and hybrid machine learning with empirical Bayesian kriging interpolation method. *Appl. Sci.* **2022**, *12*, 132.
32. Monjardin, C.E.F.; Senoro, D.B.; Magbanlac, J.J.M.; de Jesus, K.L.M.; Tabelin, C.B.; Natal, P.M. Geo-accumulation index of manganese in soils due to flooding in Boac and Mogpog Rivers, Marinduque, Philippines with mining disaster exposure. *Appl. Sci.* **2022**, *12*, 3527.

33. Wagh, V.M.; Panaskar, D.B.; Mukate, S.V.; Gaikwad, S.K.; Muley, A.A.; Varade, A.M. Health Risk Assessment of Heavy Metal Contamination in Groundwater of Kadava River Basin, Nashik, India. *Model Earth Syst. Environ.* **2018**, *4*, 969–980.
34. Kumar, S.; Toppo, S.; Kumar, A.; Tewari, G.; Beck, A.; Bachan, V.; Singh, T.B.N. Assessment of Heavy Metal Pollution in Groundwater of an Industrial Area: A Case Study from Ramgarh, Jharkhand, India. *Int. J. Environ. Anal. Chem.* **2020**, *102*, 7290–7312.
35. Abdel-Satar, A.M.; Ali, M.H.; Goher, M.E. Indices of water quality and metal pollution of Nile River, Egypt. *Egypt. J. Aquat. Res.* **2017**, *43*, 21–29.
36. Manan, T.S.B.A.; Beddu, S.; Kamal, N.L.M.; Mohamad, D.; Itam, Z.; Khan, T.; Machmudah, A.; Dutykh, D.; Mohtar, W.H.M.W.; Jusoh, H.; et al. Ecological Risk Indicators for Leached Heavy Metals from Coal Ash Generated at a Malaysian Power Plant. *Sustainability* **2021**, *13*, 10222.
37. Hoang, H.G.; Lin, C.; Chiang, C.F.; Bui, X.T.; Lukkhasorn, W.; Bui, T.P.T.; Tran, H.T.; Vo, T.D.H.; Le, V.G.; Nghiem, L.D. The individual and synergistic indexes for assessments of heavy metal contamination in global rivers and risk: A review. *Curr. Pollut. Rep.* **2021**, *7*, 247–262.
38. Senoro, D.B.; Monjardin, C.E.F.; Fetalvero, E.G.; Benjamin, Z.E.C.; Gorospe, A.F.B.; de Jesus, K.L.M.; Ical, M.L.G.; Wong, J.P. Quantitative Assessment and Spatial Analysis of Metals and Metalloids in Soil Using the Geo-Accumulation Index in the Capital Town of Romblon Province, Philippines. *Toxics* **2022**, *10*, 633.
39. de Jesus, K.L.M.; Senoro, D.B.; Natal, P.; Bonifacio, P. Groundwater Heavy Metal Contamination and Pollution Index in Marinduque Island, Philippines using Empirical Bayesian Kriging Method. *J. Mech. Eng.* **2021**, *10*, 119–141.
40. Eslami, H.; Esmaili, A.; Razaiean, M.; Salari, M.; Hosseini, A.N.; Mobini, M.; Barani, A. Potentially Toxic Metal Concentration, Spatial Distribution, and Health Risk Assessment in Drinking Groundwater Resources of Southeast Iran. *Geosci. Front.* **2022**, *13*, 101276.
41. Wu, B.; Zhao, D.Y.; Jia, H.Y.; Zhang, Y.; Zhang, X.X.; Cheng, S.P. Preliminary Risk Assessment of Trace Metal Pollution in Surface Water from Yangtze River in Nanjing Section, China. *Bull. Environ. Contam. Toxicol.* **2009**, *82*, 405–409.
42. Bortey-Sam, N.; Nakayama, S.M.M.; Ikenaka, Y.; Akoto, O.; Baidoo, E.; Mizukawa, H.; Ishizuka, M. Health Risk Assessment of Heavy Metals and Metalloid in Drinking Water from Communities near Gold Mines in Tarkwa, Ghana. *Environ. Monit. Assess.* **2015**, *187*, 397.
43. Maleki, A.; Jari, H. Evaluation of Drinking Water Quality and Non-Carcinogenic and Carcinogenic Risk Assessment of Heavy Metals in Rural Areas of Kurdistan, Iran. *Environ. Technol. Innov.* **2021**, *23*, 101668.
44. Wongsasuluk, P.; Chotpantararat, S.; Siritwong, W.; Robson, M. Heavy Metal Contamination and Human Health Risk Assessment in Drinking Water from Shallow Groundwater Wells in an Agricultural Area in Ubon Ratchathani Province, Thailand. *Environ. Geochem. Health* **2014**, *36*, 169–182.
45. Karim, Z. Risk Assessment of Dissolved Trace Metals in Drinking Water of Karachi, Pakistan. *Bull. Environ. Contam. Toxicol.* **2011**, *86*, 676–678.
46. Antoine, J.M.R.; Fung, L.A.H.; Grant, C.N. Assessment of the Potential Health Risks Associated with the Aluminium, Arsenic, Cadmium and Lead Content in Selected Fruits and Vegetables Grown in Jamaica. *Toxicol. Rep.* **2017**, *4*, 181–187.
47. Oskarsson, A. Barium. In *Handbook on the Toxicology of Metals*; Elsevier: Amsterdam, The Netherlands, 2022; pp. 91–100.
48. Ahmad, W.; Alharthy, R.D.; Zubair, M.; Ahmed, M.; Hameed, A.; Rafique, S. Toxic and Heavy Metals Contamination Assessment in Soil and Water to Evaluate Human Health Risk. *Sci. Rep.* **2021**, *11*, 17006.
49. Mishra, P.; Pandey, C.M.; Singh, U.; Gupta, A.; Sahu, C.; Keshri, A. Descriptive statistics and normality tests for statistical data. *Ann. Card. Anaesth.* **2019**, *22*, 67.
50. Monjardin, C.E.F.; de Jesus, K.L.M.; Claro, K.S.E.; Paz, D.A.M.; Aguilar, K.L. Projection of water demand and sensitivity analysis of predictors affecting household usage in urban areas using artificial neural network. In Proceedings of the 2020 IEEE 12th International Conference on Humanoid, Nanotechnology, Information Technology, Communication and Control, Environment, and Management (HNICEM), New York, NY, USA, 3–7 December 2020; pp. 1–6.
51. De Jesus, K.L.M.; Senoro, D.B.; Dela Cruz, J.C.; Chan, E.B. Neuro-particle swarm optimization based in-situ prediction model for heavy metals concentration in groundwater and surface water. *Toxics* **2022**, *10*, 95.
52. Khalid, S.; Shahid, M.; Shah, A.H.; Saeed, F.; Ali, M.; Qaisrani, S.A.; Dumat, C. Heavy metal contamination and exposure risk assessment via drinking groundwater in Vehari, Pakistan. *Environ. Sci. Pollut. Res.* **2020**, *27*, 39852–39864.
53. Schober, P.; Boer, C.; Schwarte, L.A. Correlation coefficients: Appropriate use and interpretation. *Anesth. Analg.* **2018**, *126*, 1763–1768.
54. Egbueri, J.C. Groundwater Quality Assessment Using Pollution Index of Groundwater (PIG), Ecological Risk Index (ERI) and Hierarchical Cluster Analysis (HCA): A Case Study. *Groundw. Sustain. Dev.* **2020**, *10*, 100292.
55. Ghosh, G.C.; Khan, J.H.; Chakraborty, T.K.; Zaman, S.; Kabir, A.H.M.E.; Tanaka, H. Human Health Risk Assessment of Elevated and Variable Iron and Manganese Intake with Arsenic-Safe Groundwater in Jashore, Bangladesh. *Sci. Rep.* **2020**, *10*, 5206.
56. Sharma, N.; Sodhi, K.K.; Kumar, M.; Singh, D.K. (2021). Heavy metal pollution: Insights into chromium eco-toxicity and recent advancement in its remediation. *Environ. Nanotechnol. Monit. Manag.* **2021**, *15*, 100388.
57. Garcia, A.J.; Okeagu, C.N.; Kaye, A.D.; Abd-Elsayed, A. Metabolism, Pathophysiology, and Clinical Considerations of Iron Overload, a Comprehensive Review. *Essent. Blood Prod. Manag. Anesth. Pract.* **2021**, 289–299. DOI:10.1007/978-3-030-59295-0\_28
58. Das, K.K.; Reddy, R.C.; Bagoji, I.B.; Das, S.; Bagali, S.; Mullur, L.; Khodnapur, J.P.; Biradar, M.S. Primary concept of nickel toxicity—an overview. *J. Basic Clin. Physiol. Pharmacol.* **2019**, *30*, 141–152.

59. Sachdeva, C.; Thakur, K.; Sharma, A.; Sharma, K.K. Lead: Tiny but mighty poison. *Indian J. Clin. Biochem.* **2018**, *33*, 132–146.
60. Kianoush, S.; Balali-Mood, M.; Mousavi, S.R.; Shakeri, M.T.; Dadpour, B.; Moradi, V.; Sadeghi, M. Clinical, toxicological, bio-chemical, and hematologic parameters in lead exposed workers of a car battery industry. *Iranian J. Med. Sci.* **2013**, *38*, 30.
61. Liu, B.; Lv, L.; An, M.; Wang, T.; Li, M.; Yu, Y. Heavy Metals in Marine Food Web from Laizhou Bay, China: Levels, Trophic Magnification, and Health Risk Assessment. *Sci. Total Environ.* **2022**, *841*, 156818.
62. Alfaifi, H.; El-Sorogy, A.S.; Qaysi, S.; Kahal, A.; Almadani, S.; Alshehri, F.; Zaidi, F.K. Evaluation of heavy metal contamination and groundwater quality along the Red Sea coast, southern Saudi Arabia. *Mar. Pollut. Bull.* **2021**, *163*, 111975.
63. Sajil Kumar, P.J.; Davis Delson, P.; Thomas Babu, P. Appraisal of heavy metals in groundwater in Chennai city using a HPI model. *Bull. Environ. Contam. Toxicol.* **2012**, *89*, 793–798.
64. Xu, S.; Li, S.L.; Yue, F.; Udeshani, C.; Chandrajith, R. Natural and anthropogenic controls of groundwater quality in Sri Lanka: Implications for chronic kidney disease of unknown etiology (CKDu). *Water* **2021**, *13*, 2724.
65. Snousy, M.G.; Morsi, M.S.; Elewa, A.M.; Ahmed, S.A.E.F.; El-Sayed, E. Groundwater vulnerability and trace element dispersion in the Quaternary aquifers along middle Upper Egypt. *Environ. Monit. Assess.* **2020**, *192*, 1–36.
66. Sako, A.; Bamba, O.; Gordio, A. Hydrogeochemical processes controlling groundwater quality around Bomboré gold mineralized zone, Central Burkina Faso. *J. Geochem. Explor.* **2016**, *170*, 58–71.
67. Vasileiou, E.; Papazotos, P.; Dimitrakopoulos, D.; Perraki, M. Expounding the origin of chromium in groundwater of the Sarigkiol basin, Western Macedonia, Greece: A cohesive statistical approach and hydrochemical study. *Environ. Monit. Assess.* **2019**, *191*, 509.
68. Rezaei, A.; Hassani, H.; Jabbari, N. Evaluation of groundwater quality and assessment of pollution indices for heavy metals in North of Isfahan Province, Iran. *Sustain. Water Resour. Manag.* **2019**, *5*, 491–512.
69. Çelebi, A.; Şengörür, B.; Kløve, B. Seasonal and spatial variations of metals in Melen Watershed Groundwater, Turkey. *CLEAN–Soil Air Water* **2015**, *43*, 739–745.
70. Atangana, E.; Oberholster, P.J. Using heavy metal pollution indices to assess water quality of surface and groundwater on catchment levels in South Africa. *J. Afr. Earth Sci.* **2021**, *182*, 104254.
71. Esmaeili, S.; Asghari Moghaddam, A.; Barzegar, R.; Tziritis, E. Multivariate statistics and hydrogeochemical modeling for source identification of major elements and heavy metals in the groundwater of Qareh-Ziaeddin plain, NW Iran. *Arab. J. Geosci.* **2018**, *11*, 5.
72. Duggal, V.; Rani, A.; Mehra, R.; Balaram, V. Risk assessment of metals from groundwater in northeast Rajasthan. *J. Geol. Soc. India* **2017**, *90*, 77–84.
73. Varghese, J.; Jaya, D.S. Metal pollution of groundwater in the vicinity of Valiathura sewage farm in Kerala, South India. *Bull. Environ. Contam. Toxicol.* **2014**, *93*, 694–698.
74. Karthikeyan, S.; Arumugam, S.; Muthumanickam, J.; Kulandaisamy, P.; Subramanian, M.; Annadurai, R.; Senapathi, V.; Sekar, S. Causes of heavy metal contamination in groundwater of Tuticorin industrial block, Tamil Nadu, India. *Environ. Sci. Pollut. Res.* **2021**, *28*, 18651–18666.
75. Hoang, H.G.; Chiang, C.F.; Lin, C.; Wu, C.Y.; Lee, C.W.; Cheruiyot, N.K.; Tran, H.T.; Bui, X.T. Human health risk simulation and assessment of heavy metal contamination in a river affected by industrial activities. *Environ. Pollut.* **2021**, *285*, 117414.
76. Khairudin, K.; Abu Bakar, N.F.; Ul-Saufie, A.Z.; Abd Wahid, M.Z.A.; Yahaya, M.A.; Mazlan, M.F.; Pin, Y.S.; Osman, M.S. Unravelling Anthropogenic Sources in Kereh River, Malaysia: Analysis of Decadal Spatial-Temporal Evolutions by Employing Multivariate Techniques. *Case Stud. Chem. Environ. Eng.* **2022**, *6*, 100271.
77. Topal, M.; Arslan Topal, E.I.; Öbek, E. Investigation of Potential Health Risks in Terms of Arsenic in Grapevine Exposed to Gallery Waters of an Abandoned Mining Area in Turkey. *Environ. Technol. Innov.* **2020**, *20*, 101058.
78. Yang, X.; Duan, J.; Wang, L.; Li, W.; Guan, J.; Beecham, S.; Mulcahy, D. Heavy Metal Pollution and Health Risk Assessment in the Wei River in China. *Environ. Monit. Assess.* **2015**, *187*, 111.
79. Rahaman, M.S.; Rahman, M.M.; Mise, N.; Sikder, M.T.; Ichihara, G.; Uddin, M.K.; Kurasaki, M.; Ichihara, S. Environmental arsenic exposure and its contribution to human diseases, toxicity mechanism and management. *Environ. Pollut.* **2021**, *289*, 117940.
80. Izah, S.C.; Inyang, I.R.; Angaye, T.C.; Okowa, I.P. A review of heavy metal concentration and potential health implications of beverages consumed in Nigeria. *Toxics* **2016**, *5*, 1.
81. Briffa, J.; Sinagra, E.; Blundell, R. Heavy metal pollution in the environment and their toxicological effects on humans. *Heliyon* **2020**, *6*, e04691.
82. Nickel, W.N.; Steelman, T.J.; Sabath, Z.R.; Potter, B.K. Extra-articular retained missiles; is surveillance of lead levels needed? *Mil. Med.* **2018**, *183*, e107–e113.
83. Vahidinia, A.; Samiee, F.; Faradmal, J.; Rahmani, A.; Taravati Javad, M.; Leili, M. Mercury, lead, cadmium, and barium levels in human breast milk and factors affecting their concentrations in Hamadan, Iran. *Biol. Trace Elem. Res.* **2019**, *187*, 32–40.
84. Su, J.F.; Le, D.P.; Liu, C.H.; Lin, J.D.; Xiao, X.J. Critical care management of patients with barium poisoning: A case series. *Chin. Med. J.* **2020**, *133*, 724–725.
85. Bhoelan, B.S.; Stevering, C.H.; Van Der Boog, A.T.J.; Van der Heyden, M.A.G. Barium toxicity and the role of the potassium inward rectifier current. *Clin. Toxicol.* **2014**, *52*, 584–593.
86. Yang, F.; Massey, I.Y. Exposure routes and health effects of heavy metals on children. *Biometals* **2019**, *32*, 563–573.

87. Chittick, E.A.; Srebotnjak, T. An analysis of chemicals and other constituents found in produced water from hydraulically fractured wells in California and the challenges for wastewater management. *J. Environ. Manag.* **2017**, *204*, 502–509.
88. Yuen, H.W.; Becker, W. Iron Toxicity. In *StatPearls*; StatPearls Publishing: Treasure Island, FL, USA, 2022.
89. Alharbi, O.A.; Loni, O.A.; Zaidi, F.K. Hydrochemical assessment of groundwater from shallow aquifers in parts of Wadi Al Hamad, Madinah, Saudi Arabia. *Arab. J. Geosci.* **2017**, *10*, 1–15.
90. Rehabilitation/Improvement of Mindoro East Coast Road Project. Available online: <https://documents1.worldbank.org/curated/en/709531468095354137/pdf/E14670v50EAP1EA1P079935.pdf> (accessed on 11 January 2023).
91. Chotpantarat, S.; Thamrongrisakul, J. Natural and anthropogenic factors influencing hydrochemical characteristics and heavy metals in groundwater surrounding a gold mine, Thailand. *J. Asian Earth Sci.* **2021**, *211*, 104692.
92. People Using Safely Managed Drinking Water Services (% of population)—Philippines. Available online: <https://data.worldbank.org/indicator/SH.H2O.SMDW.ZS?locations=PH> (accessed on 7 February 2023).
93. Chen, X.; Chen, W. GIS-based landslide susceptibility assessment using optimized hybrid machine learning methods. *Catena* **2021**, *196*, 104833.
94. Bui, D.T.; Van Le, H.; Hoang, N.D. GIS-based spatial prediction of tropical forest fire danger using a new hybrid machine learning method. *Ecol. Inform.* **2018**, *48*, 104–116.
95. Fanos, A.M.; Pradhan, B.; Mansor, S.; Yusoff, Z.M.; Abdullah, A.F.B. A hybrid model using machine learning methods and GIS for potential rockfall source identification from airborne laser scanning data. *Landslides* **2018**, *15*, 1833–1850.
96. Pham, B.T.; Prakash, I.; Bui, D.T. Spatial prediction of landslides using a hybrid machine learning approach based on random subspace and classification and regression trees. *Geomorphology* **2018**, *303*, 256–270.
97. Bui, D.T.; Hoang, N.D.; Nguyen, H.; Tran, X.L. Spatial prediction of shallow landslide using Bat algorithm optimized machine learning approach: A case study in Lang Son Province, Vietnam. *Adv. Eng. Inform.* **2019**, *42*, 100978.
98. Al-Ruzouq, R.; Shanableh, A.; Yilmaz, A.G.; Idris, A.; Mukherjee, S.; Khalil, M.A.; Gibril, M.B.A. Dam site suitability mapping and analysis using an integrated GIS and machine learning approach. *Water* **2019**, *11*, 1880.
99. Rahman, M.; Islam, M.; Bodrud-Doza, M.; Muhib, M.; Zahid, A.; Shammi, M.; Tareq, S.M.; Kurasaki, M. Spatio-temporal assessment of groundwater quality and human health risk: A case study in Gopalganj, Bangladesh. *Expo. Health* **2018**, *10*, 167–188.
100. Phan, K.; Phan, S.; Huoy, L.; Suy, B.; Wong, M.H.; Hashim, J.H.; Yasin, M.S.M.; Aljunid, S.M.; Sthiannopkao, S.; Kim, K.W. Assessing mixed trace elements in groundwater and their health risk of residents living in the Mekong River basin of Cambodia. *Environ. Pollut.* **2013**, *182*, 111–119.
101. Wang, L.; Li, P.; Duan, R.; He, X. Occurrence, controlling factors and health risks of Cr<sup>6+</sup> in groundwater in the Guanzhong Basin of China. *Expo. Health* **2022**, *14*, 239–251.
102. Ravindra, K.; Mor, S. Distribution and health risk assessment of arsenic and selected heavy metals in Groundwater of Chandigarh, India. *Environ. Pollut.* **2019**, *250*, 820–830.
103. Shams, M.; Tavakkoli Nezhad, N.; Dehghan, A.; Alidadi, H.; Paydar, M.; Mohammadi, A.A.; Zarei, A. Heavy metals exposure, carcinogenic and non-carcinogenic human health risks assessment of groundwater around mines in Joghatai, Iran. *Int. J. Environ. Anal. Chem.* **2022**, *102*, 1884–1899.
104. Al-Jumaily, H.A.; Mohammad, O.A.; Rasheed, B.R. Health Risk Assessment of Heavy Metals in Ground and Tap Water of Chamchamal City-Sulaymaniyah Governorate/Kurdistan Region, Iraq. *Tikrit J. Pure Sci.* **2020**, *25*, 62–70.
105. Al-Hwaiti, M.S.; Brumsack, H.J.; Schnetger, B. Heavy metal contamination and health risk assessment in waste mine water dewatering using phosphate beneficiation processes in Jordan. *Environ. Earth Sci.* **2018**, *77*, 661.
106. Zhang, W.; Ma, L.; Abuduwaili, J.; Ge, Y.; Issanova, G.; Saparov, G. Distribution characteristics and assessment of heavy metals in the surface water of the Syr Darya River, Kazakhstan. *Pol. J. Environ. Stud.* **2020**, *29*, 979–988.
107. Lim, H.S.; Lee, J.S.; Chon, H.T.; Sager, M. Heavy metal contamination and health risk assessment in the vicinity of the abandoned Songcheon Au–Ag mine in Korea. *J. Geochem. Explor.* **2008**, *96*, 223–230.
108. Li, Y.; Ma, L.; Abuduwaili, J.; Li, Y. Spatiotemporal distributions of fluoride and arsenic in rivers with the role of mining industry and related human health risk assessments in Kyrgyzstan. *Expo. Health* **2022**, *14*, 49–62.
109. Chanpiwat, P.; Lee, B.T.; Kim, K.W.; Sthiannopkao, S. Human health risk assessment for ingestion exposure to groundwater contaminated by naturally occurring mixtures of toxic heavy metals in the Lao PDR. *Environ. Monit. Assess.* **2014**, *186*, 4905–4923.
110. Kusin, F.M.; Rahman, M.S.A.; Madzin, Z.; Jusop, S.; Mohamat-Yusuff, F.; Ariffin, M. The occurrence and potential ecological risk assessment of bauxite mine-impacted water and sediments in Kuantan, Pahang, Malaysia. *Environ. Sci. Pollut. Res.* **2017**, *24*, 1306–1321.
111. Tripathee, L.; Kang, S.; Sharma, C.M.; Rupakheti, D.; Paudyal, R.; Huang, J.; Sillanpää, M. Preliminary health risk assessment of potentially toxic metals in surface water of the Himalayan Rivers, Nepal. *Bull. Environ. Contam. Toxicol.* **2016**, *97*, 855–862.
112. Abeer, N.; Khan, S.A.; Muhammad, S.; Rasool, A.; Ahmad, I. Health risk assessment and provenance of arsenic and heavy metal in drinking water in Islamabad, Pakistan. *Environ. Technol. Innov.* **2020**, *20*, 101171.
113. Rajmohan, N.; Niyazi, B.A.; Masoud, M.H. Trace metals pollution, distribution and associated health risks in the arid coastal aquifer, Hada Al-Sham and its vicinities, Saudi Arabia. *Chemosphere* **2022**, *297*, 134246.
114. Nilkarnjanakul, W.; Watchalayann, P.; Chotpantarat, S. Spatial distribution and health risk assessment of As and Pb contamination in the groundwater of Rayong Province, Thailand. *Environ. Res.* **2022**, *204*, 111838.

115. Mahmoud, M.T.; Hamouda, M.A.; Al Kendi, R.R.; Mohamed, M.M. Health risk assessment of household drinking water in a district in the UAE. *Water* **2018**, *10*, 1726.
116. Bui Huy, T.; Tuyet-Hanh, T.T.; Johnston, R.; Nguyen-Viet, H. Assessing health risk due to exposure to arsenic in drinking water in Hanam Province, Vietnam. *Int. J. Environ. Res. Public Health* **2014**, *11*, 7575–7591.
117. Benhaddya, M.L.; Halis, Y.; Hamdi-Aïssa, B. Assessment of heavy metals pollution in surface and groundwater systems in Oued Righ region (Algeria) using pollution indices and multivariate statistical techniques. *Afr. J. Aquat. Sci.* **2020**, *45*, 269–284.
118. Boum-Nkot, S.N.; Nlend, B.; Komba, D.; Ndong, G.N.; Bello, M.; Fongoh, E.J.; Ntamak-Nida, M.J.; Etame, J. Hydrochemistry and assessment of heavy metal groundwater contamination in an industrialized city of sub-Saharan Africa (Douala, Cameroon). Implication on human health. *HydroResearch* **2023**, *6*, 52–64.
119. Seleem, E.M.; Mostafa, A.; Mokhtar, M.; Salman, S.A. Risk assessment of heavy metals in drinking water on the human health, Assiut City, and its environs, Egypt. *Arab. J. Geosci.* **2021**, *14*, 1–11.
120. Endale, Y.T.; Ambelu, A.; Mees, B.; Du Laing, G. Exposure and health risk assessment from consumption of Pb contaminated water in Addis Ababa, Ethiopia. *Heliyon* **2021**, *7*, e07946.
121. Opoku, P.A.; Anornu, G.K.; Gibrilla, A.; Owusu-Ansah, E.D.G.J.; Ganyaglo, S.Y.; Egbi, C.D. (2020). Spatial distributions and probabilistic risk assessment of exposure to heavy metals in groundwater in a peri-urban settlement: Case study of Atonsu-Kumasi, Ghana. *Groundw. Sustain. Dev.* **2020**, *10*, 100327.
122. Nyambura, C.; Hashim, N.O.; Chege, M.W.; Tokonami, S.; Omonya, F.W. Cancer and non-cancer health risks from carcinogenic heavy metal exposures in underground water from Kilimambogo, Kenya. *Groundw. Sustain. Dev.* **2020**, *10*, 100315.
123. Nshimiyimana, F.X.; Faciu, M.E.; El Blidi, S.; El Abidi, A.; Soulaymani, A.; Fekhaoui, M.; Lazar, G. Seasonal influence and risk assessment of heavy metals contamination in groundwater, Arjaat village, Morocco. *Environ. Eng. Manag. J.* **2016**, *15*, 579–587.
124. Ricolfi, L.; Barbieri, M.; Muteto, P.V.; Nigro, A.; Sappa, G.; Vitale, S. Potential toxic elements in groundwater and their health risk assessment in drinking water of Limpopo National Park, Gaza Province, Southern Mozambique. *Environ. Geochem. Health* **2020**, *42*, 2733–2745.
125. Peleka, J.C.M.; Diop, C.; Foko, R.F.; Daffe, M.L.; Fall, M. Health risk assessment of trace metals in drinking water consumed in Dakar, Senegal. *J. Water Resour. Prot.* **2021**, *13*, 915–930.
126. Elumalai, V.; Brindha, K.; Lakshmanan, E. Human exposure risk assessment due to heavy metals in groundwater by pollution index and multivariate statistical methods: A case study from South Africa. *Water* **2017**, *9*, 234.
127. Idriss, I.E.; Abdel-Azim, M.; Karar, K.I.; Osman, S.; Idris, A.M. Isotopic and chemical facies for assessing the shallow water table aquifer quality in Goly Region, White Nile State, Sudan: Focusing on nitrate source apportionment and human health risk. *Toxin Rev.* **2021**, *40*, 764–776.
128. Ceballos, E.; Dubny, S.; Othax, N.; Zabala, M.E.; Peluso, F. Assessment of human health risk of chromium and nitrate pollution in groundwater and soil of the Matanza-Riachuelo River Basin, Argentina. *Expo. Health* **2021**, *13*, 323–336.
129. Rupias, O.J.B.; Pereira, S.Y.; de Abreu, A.E.S. Hydrogeochemistry and groundwater quality assessment using the water quality index and heavy-metal pollution index in the alluvial plain of Atibaia river-Campinas/SP, Brazil. *Groundw. Sustain. Dev.* **2021**, *15*, 100661.
130. Cipriani-Avila, I.; Molinero, J.; Jara-Negrete, E.; Barrado, M.; Arcos, C.; Mafla, S.; Custode, F.; Vilaña, G.; Carpintero, N.; Ochoa-Herrera, V. Heavy metal assessment in drinking waters of Ecuador: Quito, Ibarra and Guayaquil. *J. Water Health* **2020**, *18*, 1050–1064.
131. Fernández-Macias, J.C.; Ochoa-Martínez, Á.C.; Orta-García, S.T.; Varela-Silva, J.A.; Pérez-Maldonado, I.N. Probabilistic human health risk assessment associated with fluoride and arsenic co-occurrence in drinking water from the metropolitan area of San Luis Potosí, Mexico. *Environ. Monit. Assess.* **2020**, *192*, 712.
132. Avigliano, E.; Clavijo, C.; Scarabotti, P.; Sánchez, S.; Vegh, S.L.; del Rosso, F.R.; Caffetti, J.D.; Facetti, J.F.; Domanico, A.; Volpedo, A.V. Exposure to 19 elements via water ingestion and dermal contact in several South American environments (La Plata Basin): From Andes and Atlantic Forest to sea front. *Microchem. J.* **2019**, *149*, 103986.
133. Ccanccapa-Cartagena, A.; Paredes, B.; Vera, C.; Chavez-Gonzales, F.D.; Olson, E.J.; Welp, L.R.; Zyaykina, N.N.; Filley, T.R.; Warsinger, D.M.; Jafvert, C.T. Occurrence and probabilistic health risk assessment (PRA) of dissolved metals in surface water sources in Southern Peru. *Environ. Adv.* **2021**, *5*, 100102.
134. Podlasek, A.; Jakimiuk, A.; Vaverková, M.D.; Koda, E. Monitoring and assessment of groundwater quality at landfill sites: Selected case studies of Poland and the Czech Republic. *Sustainability* **2021**, *13*, 7769.
135. Kelepertzis, E. Investigating the sources and potential health risks of environmental contaminants in the soils and drinking waters from the rural clusters in Thiva area (Greece). *Ecotoxicol. Environ. Saf.* **2014**, *100*, 258–265.
136. Tiwari, A.K.; De Maio, M.; Amanzio, G. Evaluation of metal contamination in the groundwater of the Aosta Valley Region, Italy. *Int. J. Environ. Res.* **2017**, *11*, 291–300.
137. Dąbrowska, D.; Witkowski, A.J. Groundwater and Human Health Risk Assessment in the Vicinity of a Municipal Waste Landfill in Tychy, Poland. *Appl. Sci.* **2022**, *12*, 12898.
138. Dippong, T.; Hoaghia, M.A.; Mihali, C.; Cical, E.; Calugaru, M. Human health risk assessment of some bottled waters from Romania. *Environ. Pollut.* **2020**, *267*, 115409.
139. Ulniković, V.P.; Kurilić, S.M. Heavy metal and metalloid contamination and health risk assessment in spring water on the territory of Belgrade City, Serbia. *Environ. Geochem. Health* **2020**, *42*, 3731–3751.

140. Dippong, T.; Resz, M.A. Quality and Health Risk Assessment of Groundwaters in the Protected Area of Tisa River Basin. *Int. J. Environ. Res. Public Health* **2022**, *19*, 14898.
141. Kumar, S.; Islam, A.R.M.T.; Islam, H.T.; Hasanuzzaman, M.; Ongoma, V.; Khan, R.; Mallick, J. Water resources pollution associated with risks of heavy metals from Vatukoula Goldmine region, Fiji. *J. Environ. Manag.* **2021**, *293*, 112868.
142. Doaemo, W.; Betasolo, M.; Montenegro, J.F.; Pizzigoni, S.; Kvashuk, A.; Femeena, P.V.; Mohan, M. Evaluating the Impacts of Environmental and Anthropogenic Factors on Water Quality in the Bumbu River Watershed, Papua New Guinea. *Water* **2023**, *15*, 489.

**Disclaimer/Publisher's Note:** The statements, opinions and data contained in all publications are solely those of the individual author(s) and contributor(s) and not of MDPI and/or the editor(s). MDPI and/or the editor(s) disclaim responsibility for any injury to people or property resulting from any ideas, methods, instructions or products referred to in the content.